Hadamard Subtractions for Infrared Singularities in Quantum Field Theory.

George E.C. Burton

Institute for Particle & Nuclear Physics

University of Edinburgh

A thesis submitted for the degree of

Doctor of Philosophy

2010

This thesis is dedicated to the memory of my friend and supervisor
Thomas Binoth (1965-2010)

Chris: "George likes a drink-"
Thomas: "Humpf! If you did his phd you'd drink a lot too!"

Thomas made it his duty to ensure that my and every other students' time here in Edinburgh was happy, that we were enthused with our work, and that we were never short of beer, pizza and good company all of which he provided frequently with obvious pleasure. It has been a great privilege to have known him.

Declaration

All work herein is my own except where clearly referenced. No part of this work has been been submitted for any other degree or professional qualification.

George Burton,
Edinburgh 2010

Acknowledgements

Firstly I should like to thank my supervisor Tony Kennedy for the countless hours he has spent working with me on this project. I cannot adequately describing the experience of a couple of hours late one night last January in which years of our work crystallized into the identity (3.10), the week afterwards when more or less everything we have to say about Lagrange Decomposition was worked out has been the highlight of 24 years of education.

When the time came Einan Gardi immediately volunteered his assistance to supervise me in place of Thomas and I honestly don't think it would have ever been finished without his input. The enthusiasm, expertise and encouragement which he brought to this work has been invaluable and especially welcome at the time it was much needed.

Many useful discussions have come from G.Cullen, G.Heinrich, I.Wigmore, T.Kleinschmidt, T.Reiter and R.Arthur who was the first to realize the connection to Lagrange Interpolation in chapter 3.

I gratefully acknowledge the public money I have received from the STFC and the two month extension to my stipend supplied by the School of Physics.

In the last few months I have shamelessly exploited the goodwill and hospitality of many of my friends who have accommodated and entertained me, in particular I should like to thank Gavin Cullen, Sam Yoffe and Liam Keegan. Also John Danesh and Alice Jones have also put up with me for longer than I, or I imagine they, care too recall!

I can't leave Edinburgh with out mentioning the following for having made it a fantastic four years, in particular they include Daria, John R, Ben, Jamie, Tom, Simone, Laurence, Chris, Paul and many more.

Lastly I should like to thank Jane Patterson for all her patient help in ensuring that all the organization required of me to apply for, do and complete this PhD was taken as far out of my hands and into hers as possible!

Abstract

Feynman graphs in perturbative quantum field theory are replete with infrared divergences caused by the presence of massless particles, however these divergences are known to cancel order-by-order when all virtual and real contributions to a given cross section are summed and smeared against an experimental resolution. In this thesis we treat the infrared problem formally in the language of distribution theory so that we can remove the divergences with local momentum space subtractions using Hadamard's procedure. This is analogous with the BPHZ mechanism for removing UV divergences.

Our aim is to show how it is possible to make both the real and virtual subtractions analytically such that we are left with manifestly finite integrands. For the virtual graphs we present a new decomposition of the integrand in momentum space and remove those terms that are divergent. For the real graphs we show how the Taylor expansion of the momentum conserving delta function allows the explicit removal of the divergent part; furthermore we show that the homogeneous properties of the soft structure greatly simplifies this procedure.

Contents

Chapter 1

Introduction

1.1 From theory to observables

The Standard Model and other competing theories that attempt to describe fundamental physics are described by a Lagrangian, from which we can derive the equations of motion. It is the goal of particle phenomenology to use these equations to provide accurate predictions for physical observables which can be measured at collider experiments.

The equations of motions for realistic theories of nature such as QED/QCD cannot be solved exactly, however we can perform a perturbative expansion about the free-field solution which is useful for physics at high energies. To obtain an expression for the probability of some prepared incoming particles scattering into some measured out-going particles we consider these in/out particle states to be asymptotically free and calculate the overlap, known as the S-matrix. A Wick expansion of the terms in the S-matrix generates Feynman diagrams which give a graphical representation of the scattering process. A Feynman diagram is a graph whose edges denote particles, and whose vertices denote the interactions between them. An edge that links two vertices is said to be 'internal' or 'virtual' whilst an edge that is only attached to one vertex denotes a particle that is either in the initial or final state and is said to be 'external'.

The Path integral formalism [14] dictates that the probability amplitude of the evolution from an initial state to a final state is given by the sum of all possible Feynman diagrams that connect the in and out-states.

The complexity of these diagrams grows with the number of particles in the in/out states, the type of theories involved and the precision of the answer required.

1.2 Feynman Diagrams

The leading order (LO) in the perturbation series for a given process is usually given by a Feynman diagram whose graphical structure is tree-like, that is to say that there are no closed loops of particles. If the momenta of the in/out particles is known then this will uniquely specify all the momenta of any intermediate particle as well. At the next-to-leading order (NLO) Feynman graphs could be either 'virtual' or 'real emission'. A virtual graph is one with a closed loop of particles. A real emission graph features an extra massless initial/final state particle which is irresolvable from the principal external particles. In both the real emission and virtual graphs the additional particles are not detected directly and so their momentum is also unknown. We refer to the unspecified momentum as being 'free', and in both cases we are required to integrate over all possible values of free momentum to remove this parameters from the probability amplitude.

In performing the integration over the free momentum we may well encounter some or all of the three types of singularity which prevent the use of naive numerical methods, these are known as the ultraviolet (UV), the infrared (IR) and the threshold singularities.

1.2.1 Ultraviolet singularities

UV singularities occur exclusively in closed loops of virtual particles which can take arbitrarily large values of momentum. Physically these singularities are a result of our assumption that a particle is point like, that is too say the divergence that occurs for infinitely large momentum corresponds to a collision between particles over an infinitely small distance. We can crudely tame these singularities by means of a distance/energy cut-off which can be thought of as giving the particles a minimum 'size'. This alludes to some as yet unknown physics beyond the distance/energy scale that we are investigating. Having suitably regularized

the UV divergence we can then remove it by subtracting the unphysical terms from the probability amplitude. Equivalently we can think of this subtraction process as being the redefinition of the theory's parameters (masses and couplings) from the 'bare' ones that appear in the Lagrangian to the physical ones that are measured experimentally, this process is known as renormalization.

1.2.2 Infrared singularities

Infrared singularities are caused by the presence of massless particles either exchanged virtually or radiated as real emission particles, however these divergences are known to cancel order-by-order in the differential cross-section.

The asymptotic states of theories such as QED/QCD are not the same as those in the free field theory obtained by 'switching off' the interactions. In reality there is no such thing as a 'free' electron but rather it is surrounded by a cloud of soft photons, in a similar vein the asymptotic states of QCD are not free quarks but bound states of quarks and gluons.

We have already mentioned the existence of extra massless external particles that are indistinguishable from the dominant particles in the scattering event. This may occur for one of two reasons: firstly the momenta of these particles may be less (softer) than the minimum that the experimental apparatus can reliably detect; secondly the trajectory of these particles can become so parallel (collinear) to that of the dominant particle that the detector cannot resolve the angular separation between them. When evaluating higher order corrections to a given process we will consider the possibility that either of these two events could have occurred. More formally S-matrix elements and differential cross sections in Minkowski space are generalized functions which must be convolved against a suitably smooth experimental resolution that plays the role of a 'test function' to give a differential cross section. In this case we will integrate up to the point at which the massless particle becomes distinguishable from the hard event. In the soft and collinear limits of the integration the integral will diverge. Fortunately at the same order in the perturbation series there will be a virtual graph, also featuring a massless particle, which will also diverge in such a way as to cancel the divergence originating from the real emission of a massless particle.

The existence of the cancellation between infrared divergences in real emission and virtual graphs was first proved by Bloch and Nordsieck (BN) [6] for the soft divergences and by Kinoshita, Lee and Nauenberg (KLN) [21], [23] for infrared divergences in general.

1.2.3 Threshold singularities

Threshold singularities are integrable, that is to say they do not diverge, but nevertheless they provide considerable computational difficulties which have been partially overcome by deforming the integration contour. [26].

1.3 Established methods

Typically UV and IR singularities are dealt with by regularizing their divergences by altering the number of space-time dimensions from the usual 4 to some non integer $4 - 2\epsilon$. For $\epsilon < 0$ the Feynman integrals are infrared finite whilst for $\epsilon > 0$ they are UV finite, as such the ϵ allows the integration to be performed analytically. The 4 dimensional result can then obtained by expanding the solution in a Laurent series about $\epsilon = 0$. If the UV singularities can then be absorbed by a redefinition of the theory's parameters then the theory is said to be renormalizable.

The cancellation of the infrared singularities is fraught with difficulties because we expect a cancellation between divergences that exist in different phase space manifolds. The mechanism for the infrared cancellation at all orders for soft divergences was first developed in principle by Yennie, Frautschi and Suura [35] and greatly simplified by Grammer and Yennie [17]. A working, process independent, method for removing the infrared divergences in differential cross sections has proved a lot harder to develop. Today there are two main procedures: phase space slicing (PSS), and the subtraction methods [15]. One of the more popular subtraction methods, dipole subtraction [9], has been shown to be numerically the more efficient than PSS [18]. Subtraction methods work by constructing local subtraction terms in momentum space for each real emission graph. The real emission integrands and their corresponding counterterms have the same soft and

collinear limits in d-dimensions. Because the difference between the real emission graphs and the subtraction terms are explicitly point-wise convergent they can be evaluated in 4 dimensions using a Monte Carlo routine. These same subtraction terms are evaluated analytically in $4 - 2\epsilon$ dimensions so that they can be added back to the virtual graphs to preserve the overall cross section and make it finite. The subtraction terms were chosen to explicitly cancel the real divergences but also to be simple enough to allow them to be integrated analytically.

The principal drawback of this approach is the requirement to evaluate the virtual graphs analytically. The complexity of such integrals grows rapidly with the number of loops and legs, so we can only hope to find closed form solutions for the most basic loop structures. There exist procedures for reducing more complicated tensor integrals to a basis set of scalar integrals that roughly fall into two types: Feynman diagram methods, e.g. Binoth et al [4], which rely upon various forms of the tensor reduction algorithm [27]; the other approach is based upon the concept of unitarity [3].

Even after the use of such methods we are still left with the underlying basis integrals to evaluate. At one loop much of the early work was done by 't Hooft and Veltman [31] and a repository of 1-loop scalar integrals now exists [13]. Few complete graphs with more than two external particles exist at two loops. The massless double box was achieved using the promising technique of Mellin-Barnes [30] [33] but, as yet, this procedure is still limited to a few examples and does not form a general method for evaluating arbitrary loop integrals.

In spite of all the difficulties mentioned the subtraction schemes remains the most widely used mechanism for treating the infrared problem and can be considered along with the multiloop version, antenna subtraction [29], to be the state of the art.

1.4 An alternative approach to the UV

The BPH procedure for the renormalization of quantum field theory was first proposed in euclidean space by Bogoluibov and Parasiuk [7] and corrected by Hepp [19]. BPH was latter elaborated on to give the BPHZ forest formalism [36]. BPH systematically removes all UV divergences by means of a recursive

operation, this proof has been further simplified [8]. In the same way that the IR subtraction schemes make the real emission graphs infrared finite BPHZ renders any virtual graph UV finite by making local subtractions in momentum space at the level of the integrand without recourse to any regulator. The subtractions themselves are equal to the first, divergent, terms in the Taylor expansion of the original sub integrals in terms of their external momenta. BPHZ gives UV-finite momentum space integrals, which can be integrated numerically in momentum space. In order to carry out these integrals in Feynman parameter space the parametrization needs to be done consistently to avoid numerical problems [20].

1.5 An alternative approach to the IR?

The great appeal of methods such as BPHZ and the IR subtraction schemes is that they are automatic. They work at the level of the integrand and because they require no regulation it is simple to perform the integration itself numerically. The use of the IR subtraction schemes for real emission integrals is straight-forward but the use of BPHZ for virtual graphs is not because there are still infrared virtual divergences. The premise of this PhD is to establish if it is possible to develop an additional procedure that removes the remaining infrared divergences from the virtual graphs using local momentum subtractions - this new technique when used in conjunction with BPHZ should enable us to automatically render the whole cross section finite to facilitate numerical evaluation.

To simplify the task we shall restrict ourselves to the soft infrared divergences and ignore the collinear ones.

As it is well known that the generalized eikonal approximation captures the full soft behavior of an arbitrary Feynman graph, our first attempt at making a soft subtraction was simply to subtract this approximation from the original graph. It is one task to make a subtraction from an integrand but it is quite another to evaluate the difference between the two integrals. The usual technique for evaluating Feynman integrals is to use Feynman parametrization to turn the integrand into a quadratic form so that the virtual momentum integral can be performed analytically this leaves us with multiple Feynman parameter integrals

to evaluate. For the BPHZ procedure it is fortunate that Feynman parametrization preserves the UV pole structure such that the divergences in the original integrand and in the subtraction terms cancel in α space, however this is not the case for the infrared pole structure.

To overcome what appears to be merely a technical obstacle in an otherwise sound procedure we force the cancellation between the integrand and the infrared subtraction by cross multiplying the terms in the denominator. This converts two (or more) divergent integrands into one (or more) convergent integrands. As the resulting integrands are manifestly convergent, it should be possible to evaluate them individually using the usual techniques such as Feynman parametrization.

Surprisingly we have come across a remarkably elegant formulation of the procedure outlined above which we present in chapter 3. This procedure is explicitly based upon the theory of the regularization of generalized functions and the analytic structure of the Feynman graph.

The numerical evaluation of the subtracted real emission graphs is simple but unfortunately, in spite of all our efforts to make the integrand explicitly finite, the same is not true of the subtracted virtual graphs. The problem lies in the convergence criteria of the Feynman parameter integrals. In chapter 4 we shall investigate exactly what these criteria are. Numerical instabilities are caused by the physical singularities that correspond to the possibility that pairs of virtual particles can become 'real'. For the bubble, triangle and box graph we have a procedure for 'rotating' these thresholds away from the contour of integration such that the integral can be performed numerically.

The IR subtraction schemes start by constructing subtraction terms specifically engineered to easily cancel against the real emission graphs in the soft limit but our method is based upon finding subtractions that render the virtual graphs finite - these subtractions are not the same as those found in the IR subtraction schemes and it is not trivial to make them cancel against the real emission graphs in the soft limit. Again we find ourselves in the position of having to calculate the difference of two divergent integrands that we know must be finite when integrated together but lacking the technology to make this happen. In chapter 5 we investigate how we can force the cancellation of the real graphs and their corresponding subtractions as we did for the virtual ones. Again we shall appeal to

the theory of generalized functions to work out how to take the difference of two delta functions. Yet again we are rewarded with a another surprisingly simple result that is a consequence of the conformal invariance of the soft structure.

Unfortunately we have not been able to derive a general formulation for the rotation of the physical poles for arbitrary graphs and we are still unable to cope with the physical singularities that remain when we make subtractions from the virtual graphs. In chapter 7 we start by speculating that there could be an analogue of the phase-space-slicing technique for virtual graphs and indeed we do find one but it turns out to be more complicated than the full calculation. However the tools developed along the way are interesting in their own right and shed some more light on numerical treatments of the singular structure. We begin by supposing that rather than regulate the soft divergences with a mass regulator we could in fact use a non zero value of $i\epsilon$. We then suppose that rather than attempt to extrapolate to ever smaller values of $i\epsilon$ we could calculate the solution for a 'large' value and work out the difference. The motivation for this approach is that, for the graphs attempted at least, this difference turns out to be particularly simple to calculate. In fact we can use this approach to recover the full analytic solution using nothing more that the integration routines found in Mathematica [34] and avoiding the use of specialist knowledge of dispersion integrals as used in the original calculations [31]. This chapter represents something of a departure from the rest of the thesis and can viewed as an appendix to the main results.

Before attempting to discover new subtraction methods we shall begin by revisiting the theory of the cancellation of soft divergences. There is an interesting contrast between these two cancellation theories: KLN requires that both initial and finite degenerate states are summed over whereas BN only requires that the final states are considered. This has already been questioned and it has been suggested that should soft initial states be considered on the same footing as soft final states in the manner of KLN then the canonical cancellation of infrared divergences fails [22]. This is investigated in Chapter 2.

Chapter 2

Time reversible Bloch-Nordsiek cancellation

2.1 Introduction

Both virtual and real emission Feynman diagrams featuring massless particles can have infrared singularities that give rise to infinite quantities.

Bloch and Nordsieck (BN) showed that apparent infrared singularities cancel between virtual and real emission graphs if we test our differential cross section against a sufficiently smooth experimental resolution [6].

One should ask how this cancellation behaves under time reversal, after all we cannot fix exactly the energy of the initial state any more that we can exactly measure the energy of the final state. The integral over arbitrarily soft incoming radiation should diverge by symmetry but apparently there is nothing left to cancel against.

Indeed it has been argued that the soft incoming radiation graph is a valid contribution to the overall cross section and that as such it should be added to the usual sum of virtual and real emission graphs. This would imply that the BN procedure does not render the overall cross section finite and that our understanding of infrared cancellations is incomplete [22].

Our goal is to resolve this apparent contradiction by showing that the time asymmetry is built in the limiting procedure used to define the phase space aver-

aging and that the only physically unambiguous procedure is to sum the in/out phase space contributions.

2.2 Example of the cancellation of soft divergences

Let us consider the decay of an off-shell massless particle into two massive particles in four dimensions, which at leading order (LO), is matrix element represented by the tree-level graph in fig. 2.1. In this toy theory the Feynman rules are $-i\lambda$ for vertices, $\frac{i}{p^2-m^2+i\epsilon}$ for propagators with momentum p and mass m and $\delta^{\pm}(p^2-m^2)$ for radiated on-shell particles with positive/negative energy p^0 and mass m. At next-to-leading order (NLO) the full matrix element consists of three

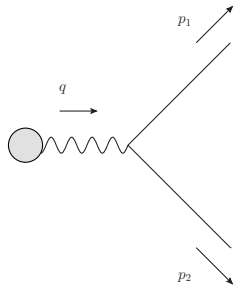

Figure 2.1: Leading order approximation for an off-shell massless particle into two massive particles.

virtual graphs fig. 2.2, and two real graphs fig. 2.3. The matrix elements are,

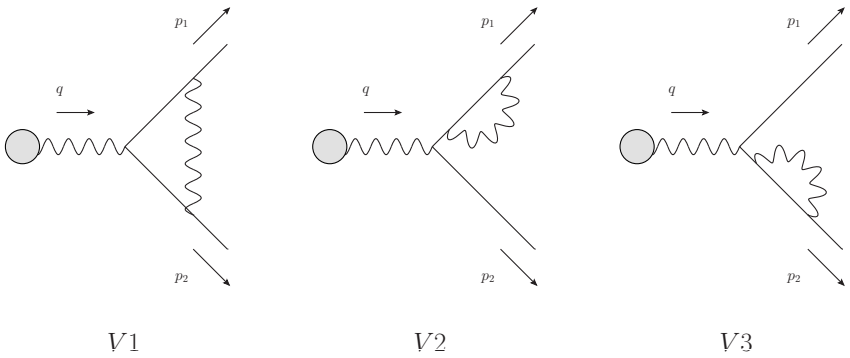

Figure 2.2: Virtual corrections to fig. 2.1.

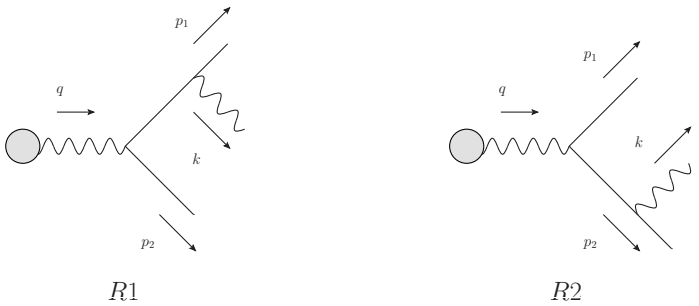

Figure 2.3: Real emission corrections to fig. 2.1.

$$
\begin{aligned}
V1 &= (i\lambda)^3 \int \frac{d^4k}{(2\pi)^4} \frac{i}{k^2 + 2k\cdot p_1 + i\epsilon} \frac{i}{k^2 - 2k\cdot p_2 + i\epsilon} \frac{i}{k^2 + i\epsilon} \\
V2 &= (i\lambda)^3 \; Z^{-1/2} \int \frac{d^4k}{(2\pi)^4} \frac{i}{k^2 + 2k\cdot p_1 + i\epsilon} \frac{i}{k^2 + i\epsilon} \\
V3 &= (i\lambda)^3 \; Z^{-1/2} \int \frac{d^4k}{(2\pi)^4} \frac{i}{k^2 - 2k\cdot p_2 + i\epsilon} \frac{i}{k^2 + i\epsilon}
\end{aligned} \tag{2.1}
$$

for the virtual graphs[1] fig. (2.2) and,

$$
\begin{aligned}
R1 &= (i\lambda)^2 \frac{i}{k^2 + 2k\cdot p_1 + i\epsilon} \\
R2 &= (i\lambda)^2 \frac{i}{k^2 + 2k\cdot p_2 + i\epsilon},
\end{aligned} \tag{2.2}
$$

for the real graphs.

The full cross section is the sum of the matrix elements squared integrated against the relevant Lorentz-invariant phase-space, L, and a smooth experimental resolution which plays the role of a test function. At NLO we have:

$$
\sigma_{\text{NLO}} = \sigma_{\text{LO}} + \sigma_{\text{virtual 1}} + \sigma_{\text{virtual 2}} + \sigma_{\text{virtual 3}} + \sigma_{\text{real 1}} + \sigma_{\text{real 2}} + \sigma_{\text{real 3}} + \mathcal{O}(\lambda^6) \tag{2.3}
$$

The full expressions for the contributions to the cross section are given by the following,

$$
\sigma_{\text{Born}} = \lambda^2 \int L_{1\to 2}, \tag{2.4}
$$

[1] The factor $Z^{-1/2}$ appearing in the self energy graphs account for the wave function renormalization in place of the infinite quantity $\frac{i}{p^2 - m^2 + i\epsilon}$.

$$\begin{aligned}
\sigma_{\text{virtual 1}} &= -\lambda^4\, 2\Re\left[\int \frac{d^4k}{(2\pi)^4}\,\frac{i}{k^2+2k\cdot p_1+i\epsilon}\frac{i}{k^2-2k\cdot p_2+i\epsilon}\frac{i}{k^2+i\epsilon}\right] L_{1\to 2}\\
\sigma_{\text{virtual 2}} &= -\lambda^4\, Z^{-1/2}\,\Re\left[\int \frac{d^4k}{(2\pi)^4}\,\frac{i}{k^2+2k\cdot p_1+i\epsilon}\frac{i}{k^2+i\epsilon}\right] L_{1\to 2}\\
\sigma_{\text{virtual 3}} &= -\lambda^4\, Z^{-1/2}\,\Re\left[\int \frac{d^4k}{(2\pi)^4}\,\frac{i}{k^2-2k\cdot p_2+i\epsilon}\frac{i}{k^2+i\epsilon}\right] L_{1\to 2}
\end{aligned} \tag{2.5}$$

$$\begin{aligned}
\sigma_{\text{real 1}} &= \lambda^4\, 2\Re\int\left[\frac{i}{2k\cdot p_1+i\epsilon}\frac{i}{-2k\cdot p_2+i\epsilon}\right] L_{1\to 3}\\
\sigma_{\text{real 2}} &= \lambda^4\,\Re\int\left[\frac{i}{2k\cdot p_1+i\epsilon}\right]^2 L_{1\to 3}\\
\sigma_{\text{real 3}} &= \lambda^4\,\Re\int\left[\frac{i}{-2k\cdot p_2+i\epsilon}\right]^2 L_{1\to 3}
\end{aligned} \tag{2.6}$$

Lorentz-invariant phase space terms for the decay of one particle into a massive electron-positron pair and possibly an additional massless particle are:

$$\begin{aligned}
L_{1\to 2} &= \delta^+(p_1^2-m_1^2)\delta^+(p_2^2-m_2^2)(2\pi)^4\delta^4(q-p_1-p_2)\, f(p_1,p_2,0)\\
&\qquad \frac{d^4p_1}{(2\pi)^3}\,\frac{d^4p_2}{(2\pi)^3}\\
L_{1\to 2+\gamma} &= \delta^+(p_1^2-m_1^2)\delta^+(p_2^2-m_2^2)\delta^+(k^2)(2\pi)^4\delta^4(q-p_1-p_2-k)\, f(p_1,p_2,k)\\
&\qquad \frac{d^4p_1}{(2\pi)^3}\,\frac{d^4p_2}{(2\pi)^3}\,\frac{d^4k}{(2\pi)^3}
\end{aligned} \tag{2.7}$$

where f is a smooth function specifying the experimental resolution, and,

$$\delta^{\pm}(p^2-m^2) = \theta(\pm p^0)(2\pi)\delta(p^2-m^2). \tag{2.8}$$

We note that the leading order contribution and the virtual contribution are manifestly time symmetric in k but that the real emission contribution is not. This is due to the presence of a Heaviside step function in the phase-space expression for the emission of the massless particle. In the following section we shall make the usual assumption there are only soft out-going massless particles and show that

the expected cancellation between real and virtual processes does take place. In § 2.4 we shall use a mass regulator to explore whether we can distinguish between arbitrarily soft in-coming and out-going particles and conclude that we cannot.

2.3 Infrared cancellation

All the graphs at $\mathcal{O}(\lambda^4)$ are divergent in the soft limit $k \to 0$. Unitarity guarantees that for a given process all infrared divergences from contributing real and virtual graphs at a given order will cancel when integrated against a smooth test function. More specifically the cutting equations [11] show how the cancellation of divergences will take place between $\sigma_{\text{virtual }1}$ and $\sigma_{\text{real }1}$, between $\sigma_{\text{virtual }2}$ and $\sigma_{\text{real }2}$, and between $\sigma_{\text{virtual }3}$ and $\sigma_{\text{real }3}$. We shall explicitly show how this cancellation works in the first case.

If we subtract from $\sigma_{\text{real }1}$ the following integral known as the eikonal approximation,

$$\sigma_{\text{eikonal}} = \lambda^4\, 2\Re \int \frac{d^4k}{(2\pi)^4} \left[\frac{i}{2k\cdot p_1 + i\epsilon}\frac{i}{-2k\cdot p_2 + i\epsilon}\right] \delta^+(k^2)\, L_{1\to 2}, \tag{2.9}$$

then we have another integral which is convergent in the soft limit $k \to 0$:

$$\begin{aligned}\text{finite}[\sigma_{\text{real }1}] = \lambda^4\, 2\Re \int \frac{d^4k}{(2\pi)^4} &\left[\frac{i}{2k\cdot p_1 + i\epsilon}\frac{i}{-2k\cdot p_2 + i\epsilon}\right] \\ &\times \delta^+(k^2)\delta^+(p_1^2 - m_1^2)\delta^+(p_2^2 - m_2^2) \\ &\times \left[\delta(q - p_1 - p_2 - k)\, f(p_1, p_2, k) - \delta(q - p_1 - p_2)\, f(p_1, p_2, 0)\right] d^4p_1\, d^4p_2.\end{aligned}$$

Note that the $f(p_1, p_2, 0)$ term in the last line above comes from the two body phase-space expression in the eikonal approximation (2.9). Alternatively we can also rewrite (2.9) by constructing the real part as the sum of the matrix element squared plus its complex conjugate,

$$\sigma_{\text{eikonal}} = \lambda^4 \int \frac{d^4k}{(2\pi)^4} \left[\frac{i}{2k\cdot p_1 + i\epsilon}\frac{i}{-2k\cdot p_2 + i\epsilon} + \frac{-i}{2k\cdot p_1 - i\epsilon}\frac{-i}{-2k\cdot p_2 - i\epsilon}\right] \delta^+(k^2)\, L_{1\to 2}. \tag{2.10}$$

Using the fact the integration measure is invariant under the following transformation,

$$k \to -k, \tag{2.11}$$

we have,

$$\sigma_{\text{eikonal}} = \lambda^4 \int \frac{d^4k}{(2\pi)^4} \frac{i}{2k\cdot p_1 + i\epsilon} \frac{i}{-2k\cdot p_2 + i\epsilon} 2\pi\delta(k^2)\, L_{1\to 2}. \tag{2.12}$$

In this form we see that the eikonal subtraction, (2.12), is also time reversible in the manner of (2.4) and (2.5). Using the well known result from the theory of generalized functions,

$$2\pi\delta(x) = \lim_{\epsilon\to 0}\left(\frac{i}{x+i\epsilon} + \frac{-i}{x-i\epsilon}\right), \tag{2.13}$$

we can rewrite the phase-space expression for the emission of a particle $\delta(k^2)$ as the real part of a propagator for virtual particle,

$$\sigma_{\text{eikonal}} = \lambda^4 \int \frac{d^4k}{(2\pi)^4} \frac{i}{2k\cdot p_1 + i\epsilon} \frac{i}{-2k\cdot p_2 + i\epsilon} \left[\frac{i}{k^2+i\epsilon} + \frac{-i}{k^2 - i\epsilon}\right] L_{1\to 2} \tag{2.14}$$

$$= \lambda^4\, 2\Re \int \frac{d^4k}{(2\pi)^4} \left[\frac{i}{2k\cdot p_1 + i\epsilon} \frac{i}{-2k\cdot p_2 + i\epsilon} \frac{i}{k^2+i\epsilon}\right] L_{1\to 2}. \tag{2.15}$$

where again we have made use of (2.11). Subtracting this virtual form of σ_{eikonal} from $\sigma_{\text{virtual 1}}$ we have another integrand that converges in the soft limit,

$$\text{finite}[\sigma_{\text{virtual 1}}] = -\lambda^4\, 2\Re \int d^4k \left(\frac{i}{k^2 + 2k\cdot p_1 + i\epsilon} \frac{i}{k^2 - 2k\cdot p_2 + i\epsilon} - \frac{i}{2k\cdot p_1 + i\epsilon} \frac{i}{-2k\cdot p_2 + i\epsilon}\right) \frac{i}{k^2+i\epsilon} L_{1\to 2} \tag{2.16}$$

What we have explicitly shown above is that we can subtract an infinite contribution from one part of the cross section in order to make it finite and then add back the same infinite quantity to another part of the cross section to make that finite as well without changing the overall result.

We can show the same cancellation between the remaining divergent inte-

grands once we have renormalized the self-energy graphs in fig. 2.2.

2.4 Mass Regulator

It is illuminating to consider the analogous phase space computation in the situation with a very light particle with a mass μ. The only significant difference is that the three particle phase space can be split into disjoint positive and negative energy pieces using the identity,

$$\delta(k^2-\mu^2) = \delta^+(k^2-\mu^2) + \delta^-(k^2-\mu^2) = \frac{\delta(k_0-\omega)}{2\omega} + \frac{\delta(k_0+\omega)}{2\omega} \tag{2.17}$$

where $\omega = \sqrt{|\vec{k}|^2+\mu^2}$. For $\mu \neq 0$ it is possible in principle for the light particles in the initial or final state to be resolved experimentally. The soft contribution to the real emission, absorption and virtual graphs is then given by the eikonal approximation (2.12) modified by a small mass μ which then grows as $\ln(\mu/m)$ for $\mu \ll m$.

$$\sigma_{\text{Light 'eikonal'}} = \lambda^4 \int \frac{d^4k}{(2\pi)^4} \frac{i}{\mu^2 + 2k\cdot p_1 + i\epsilon} \frac{i}{\mu^2 - 2k\cdot p_2 + i\epsilon} 2\pi\delta(k^2-\mu^2)\, L_{1\to 2}. \tag{2.18}$$

This shows that there are (logarithmically) large[1] contributions to the differential cross section corresponding to the three experimentally distinguishable cases where a soft light particle is emitted, absorbed, or neither. The emission and absorption of soft light particles is enhanced at the expense of the case where there are no soft light particles in either the initial or final state.

If the experimental resolution is not sufficient to distinguish between these cases then the (smeared) cross section does not show this behavior. The magnitude of this "inclusive" cross section could still be large, but its magnitude does not diverge as $\mu \to 0$, instead it depends upon the derivative of the experimental resolution $\partial f/\partial k_\mu$.

[1] We assume that $\lambda^2 \ln(\mu/m) \ll 1$ so that the next-to-leading order contributions to the cross section are small compared to the leading-order Born contribution, as otherwise the naïve perturbation expansion would not be valid.

2.5 The Equation of Greatest Time

't Hooft and Veltman use the following expression to show how the poles of the virtual and real 'cut' propagators cancel [32],

$$\Delta_F(x_2 - x_1) + \Delta_F^\star(x_2 - x_1) - \Delta^+(x_2 - x_1) - \Delta^-(x_2 - x_1) = 0 \tag{2.19}$$

The expressions that contribute to (2.19) all denote various ways one particle can propagate between two space-time points, x_1 and x_2. We can separate this into both (all) time orderings by recalling that the propagator is defined by the Feynman prescription,

$$\Delta_F(x) = \theta(x_2^0 - x_1^0)\,\Delta^+(x_2 - x_1) + \theta(x_1^0 - x_2^0)\,\Delta^-(x_2 - x_1) \tag{2.20}$$

where[1],

$$\Delta^\pm(x) = \int \frac{d^4p}{(2\pi)^3}\, e^{-ip\cdot(x_2 - x_1)}\, \theta(\pm p^0)\, \delta(p^2 - m^2). \tag{2.21}$$

Furthermore we can trivially partition the cut propagators into the two time orderings using the fact that $1 = \theta(x_1^0 - x_2^0) + \theta(x_2^0 - x_1^0)$. It is now clear that (2.19) is true for each of possibilities $x_1^0 > x_2^0$ and $x_1^0 < x_2^0$ individually. This is a special case of 'The Equation of Greatest Time' [32].

In § 2.3 we presumed that the emitted soft particle was radiated into the final state, we could have been more precise by modifying (2.8) to be,

$$\delta^\pm(p^2 - m^2) = 2\pi\theta(\pm p^0)\theta(\pm x^0)\delta(p^2 - m^2), \tag{2.22}$$

this appears to be rather heavy handed because we usually assume that the asymptotic states are unambiguously either in the far-future or the distant-past but for massless particles this is not so: how can we make a claim about the timing of a particle that we did not detect?

We suggest that the expression for phase-space of a soft particle, i.e. (2.7)

[1] Notation is taken from [32] adapted for difference in the metric.

should be modified as,

$$L_{1\to 2+\gamma} = \delta^+(p_1^2 - m_1^2)\delta^+(p_2^2 - m_2^2)2\pi\delta(k^2)[\theta(+k^0)\theta(+x^0) + \theta(-k^0)\theta(-x^0)] \\ \times\ \delta^4(q - p_1 - p_2 - k)\, f(p_1, p_2, k)\, d^4p_1\, d^4p_2\, d^4k, \tag{2.23}$$

in accordance with the Feynman prescription. This modified phase-space term allows for both the possibility of real emission and absorption on an equal footing. In order to show that this reproduces the original BN cancellation in a time symmetric way it is necessary to split the expression for the cross section for the absorption/emission of a massless particle with momentum k into an infrared finite piece which is anti-symmetric in $k \to -k$ and into a divergent piece which, like the cross section for the virtual graph, is symmetric. For the example considered before this is easily done by writing,

$$\Delta(k) = (2\pi)^4\delta^4(q - p_1 - p_2 - k)\, f(p_1, p_2, k), \tag{2.24}$$

as,

$$\Delta(k) = \Delta_{\text{anti}}(k) + \Delta_{\text{sym}}(k). \tag{2.25}$$

where,

$$\Delta_{\text{anti}}(k) := \Delta(k)/2 - \Delta(-k)/2, \tag{2.26}$$

and,

$$\Delta_{\text{sym}}(k) := \Delta(k)/2 + \Delta(-k)/2. \tag{2.27}$$

For example the divergent part of the $\sigma_{\text{real }1}$ is now,

$$\text{divergent}[\sigma_{\text{real }1}] = \lambda^4 \int \frac{i}{2k\cdot p_1 + i\epsilon}\frac{i}{-2k\cdot p_2 + i\epsilon} 2\pi\delta(k^2)\left[\theta(+x^0) + \theta(-x^0)\right] \\ \times \delta^+(p_1^2 - m_1^2)\delta^+(p_2^2 - m_2^2)\Delta_{\text{sym}}(k)\, d^4p_1\, d^4p_2, \tag{2.28}$$

which cancels against the eikonal approximation (2.12) in the soft limit irrespective of whether soft radiation is either emitted $x^0 > 0$ or absorbed $x^0 < 0$ as the

following expression,

$$\Delta_{\text{sym}}(k) - (2\pi)^4\delta^4(q - p_1 - p_2)\ f(p_1, p_2; 0) \tag{2.29}$$

tend to zero in the soft limit.

2.6 Conclusions

We see from the calculations of the preceding sections that if a particle has a tiny mass then there is a logarithmically large contribution to the cross section from real absorption, and a corresponding large virtual contribution. If we can resolve whether k_0 is positive, negative, or zero, then these large contributions are physically observable. However if the experimental apparatus cannot resolve whether a light particle is incoming or outgoing then these large contributions cancel.

If the emitted particle is massless then we cannot even in principle distinguish incoming from outgoing massless particles if they are sufficiently soft, and there is no observable infrared singularity.

It is usual to assume that the energy-momentum q of the initial state is prepared exactly, and that the difference between the initial and final state energy $(q - p_1 - p_2)_0 \geq 0$ is lost to undetected soft massless particles in the final state. We argue that physically we can no more prepare the initial state momentum exactly than we can detect the final state momenta exactly. For sufficiently soft massless particles it is impossible to tell whether they are incoming or outgoing. One may consider the incoming state to contain a sea of soft particles, just as the outgoing state does.

It has been argued [22] that because there is no extra virtual divergence to cancel against the extra incoming divergence the standard cancellation picture mechanism is incomplete. In fact there is no 'extra' divergence in the initial state to worry about, rather this divergence is indivisible from the usual final state emission amplitude.

Chapter 3

Lagrange Decomposition

3.1 Introduction

In the previous chapter we introduced the notion of the soft infrared divergence that is induced by the presence of massless particles that are either exchanged virtually or absorbed/emitted as real particles. We tidied up some of the subtleties involved with step functions to make the real radiation graphs symmetric in both x and k space in the soft limit just as it is for the virtual graphs. We also noted that the soft limit for the real graphs is equal (and opposite in sign) to the soft limit for the virtual graphs therefore divergences cancel in the full cross section. This chapter is concerned with making that cancellation manifest for the virtual graphs.

BPHZ removes UV divergences from virtual graphs by means of local momentum space subtractions, likewise IR subtraction methods remove infrared divergences from real graphs also by means of local momentum space subtractions. If we develop an analogous system of subtractions to remove the infrared divergences from virtual graphs using local momentum space subtractions then we will have a complete set of procedures to make an integrand finite without using a regulator and we will be able to compute the integral directly using a Monte Carlo routine in four dimensions.

Another compelling reason to use numerical methods is that the Feynman amplitude will have to be convolved against an appropriate experimental resolution to obtain a testable prediction. This convolution will inevitably be performed

by Monte Carlo so the business of making a physical prediction is unavoidably numerical in nature. We propose that we may as well use a numerical approach throughout the calculation which would place the calculation of virtual graphs on an equal footing with the calculation of the real ones.

Should we succeed in finding a method for removing infrared singularities that is as general as BPHZ is for UV singularities then we will have found a numerical method for calculating any perturbative cross section to any order.

Our first idea was to simply take a graph (renormalized by BPHZ) and then subtract from it its generalized eikonal approximation to remove its soft singularities. We reasoned that so long as we Feynman parametrized the integral and its subtraction consistently then then the soft singularities would cancel point-wise in parameter space. Unfortunately Feynman parametrization does not locally preserve the soft structure found in momentum space and so there is no local cancellation found between the corresponding parameter space integrands.

Frustrated by what appears to be a technical failure in the implementation of an otherwise sound idea we wondered if we could force the cancellation of the divergences analytically before integrating. Such a method would produce a manifestly finite integrand which must converge irrespective of the details of the parametrization. As an example we shall consider the expression for the difference between the virtual triangle graph and the corresponding eikonal subtraction (2.16) from the last chapter which we shall rewrite with only the essential part as,

$$\int d^4k \left(\frac{1}{k^2 + 2k \cdot p_1 + i\epsilon} \frac{1}{k^2 - 2k \cdot p_2 + i\epsilon} - \frac{1}{2k \cdot p_1 + i\epsilon} \frac{1}{-2k \cdot p_2 + i\epsilon} \right) \frac{1}{k^2 + i\epsilon}, \tag{3.1}$$

the cancellation of the divergences can now be forced by cross multiplying,

$$- \int d^4k \, \frac{k^2 + 2k \cdot p_1 - 2k \cdot p_2}{[k^2 + 2k \cdot p_1 + i\epsilon][k^2 - 2k \cdot p_2 + i\epsilon][2k \cdot p_1 + i\epsilon][-2k \cdot p_2 + i\epsilon]}. \tag{3.2}$$

Ignoring the fact that the eikonal approximation, and hence the expression above, are both UV divergent we can still see that it is soft finite in 4-dimensions. Furthermore the numerator can be rewritten in terms of inverse propagators which can be canceled by those in the denominator.

Much effort has been spent trying to generalize the procedure outlined above to more complicated graphs with multiple soft particles and multiple loops, using smooth partitions in momentum space to separate the various overlapping soft divergences. However complicated the graph our approach had always been the same: identify the various soft limits for a given integrand; subtract them from the original integrand such that the massless particles 'cancel'; and present the result in the most 'symmetric' way possible.

Serendipitously we have came across an elegant reformulation of this procedure whilst considering a different (but related) issue. This new approach allows an easy derivation of the full result for a generic graph and is called Lagrange Decomposition. The central identity is given by (3.10) which we will examine in detail throughout this chapter.

Lagrange decomposition was discovered whilst trying to remove threshold singularities from the bubble graph fig. 3.1. A threshold singularity occurs when

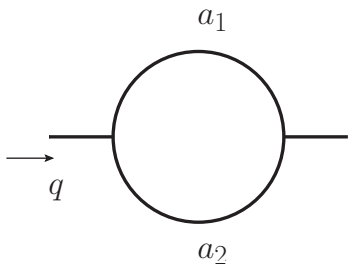

Figure 3.1: A bubble graph with all lines massive.

two or more propagators become on-shell simultaneously for a particular value of the loop momentum. In a bubble graph this means that all propagators are on-shell. We reasoned that if we were to make a subtraction for the limit where each propagator became on-shell we would succeed in removing all singularities.

The integrand for the bubble graphs is:

$$I_2 = \frac{i}{(k+q)^2 - m^2 + i\epsilon} \frac{i}{k^2 - m^2 + i\epsilon}, \tag{3.3}$$

where q is the incoming momentum and k is the free loop momentum. To remove the singularity originating with the first propagator becoming on shell we subtract

from the integrand a term comprised of the first propagator multiplied by the second in the limit that the first becomes singular, i.e. $(k+q)^2 = m^2 + i\epsilon$,

$$I_2 - \frac{i}{(k+q)^2 - m^2 + i\epsilon} \frac{i}{-2k\cdot q - q^2}. \tag{3.4}$$

Making an equivalent subtraction for the second divergence gives us the following,

$$\text{finite}[I_2] := I_2 - \frac{i}{(k+q)^2 - m^2 + i\epsilon} \frac{i}{-2k\cdot q - q^2} - \frac{i}{2k\cdot q + q^2} \frac{i}{k^2 - m^2 + i\epsilon}. \tag{3.5}$$

As hoped for this procedure does indeed remove all singularities from the integrand but not in the manner we had intended, in fact (3.5) is equal to zero. It turns out that this procedure is completely general and that for any loop integral making a subtraction about each and every propagator becoming on-shell will render the integrand identically zero. As a method for coping with threshold singularities this has not proved to be a particularly fruitful avenue of research but it suggests an intriguing approach for coping with the soft singularities.

If we take a divergent graph and rewrite it as the sum of all possible subtractions we can separate those that are divergent from those that are finite. The subtractions that are finite can be evaluated numerically whilst the divergent subtractions can be isolated from the numerical calculation. It is the purpose of this chapter to explain how exactly this can work.

3.1.1 Outline of chapter

Before we apply Lagrange decomposition to some practical calculations in § 3.6 we shall first investigate its connections to other key ideas.

Firstly in § 3.2 we shall derive the fundamental identity (3.10) systematically using the Lagrange interpolation polynomials (hence the name). From here it is then clear how Lagrange decomposition is naturally related to Hadamard's prescription for the regularization of generalized functions which we introduce and explain in § 3.3. We also need to bear in mind that we are calculating a physical process and as such we must make a connection to the real graphs. The cutting equations show that all graphs, real and virtual, have an identical

singularity structure. In § 3.4 we shall explore a clear link between Lagrange decomposition and the cutting equations.

We also note that Lagrange decomposition reduces a divergent integrand featuring massless propagators to one which does not. To what extent this can be used as a basis for a proof that the remaining integrand is formally finite is investigated in § 3.5.

Lastly it is instructive to map Lagrange decomposition to parameter space to show its relation to another decomposition technique, Sector-Decomposition, which is done in § 3.7.

3.2 Lagrange Interpolation

The Lagrange interpolation method is a result from numerical analysis that fits a polynomial, $L(x)$, to a set of data points $\{f(x_i), i = 1..n\}$. L is given by

$$L(x) = \sum_{i=1}^{n} f(x_i) l_i(x) \tag{3.6}$$

where,

$$l_i(x) = \prod_{j=1, j\neq i}^{n} \frac{x - x_j}{x_i - x_j} \tag{3.7}$$

If we use this to fit a polynomial to the constant $f(x) = 1$ then we have,

$$1 = \sum_{i=1}^{n} \prod_{j\neq i}^{n} \frac{x - x_j}{x_i - x_j}. \tag{3.8}$$

Which can be rewritten in terms of a new variable, $A_i = x - x_i$, to generate a partition of unity,

$$1 = \sum_{i=1}^{n} \prod_{j\neq i}^{n} \frac{A_j}{A_j - A_i} \tag{3.9}$$

Finally we multiply by $\prod_{j=1}^{n} \frac{1}{A_j}$ to get the key identity (3.10).

$$\prod_{i=1}^{n} \frac{1}{A_i} = \sum_{i=1}^{n} \frac{1}{A_i} \prod_{j\neq i}^{n} \frac{1}{A_j - A_i} \qquad \forall n \in \mathbb{Z}^+ \tag{3.10}$$

An alternative proof of this identity can be found in appendix A.

3.3 Hadamard's Proceedure

This section begins with a somewhat abstract treatment of divergent functions as distributions. We shall see how to extract the finite part from such distributions by means of an appropriate subtraction known as Hadamard's procedure.

Consider an integral of a function which is divergent at a point x_0 multiplied by another function ϕ which is infinitely differentiable at x_0. Furthermore ϕ has either compact support or all of its derivatives tend to zero more rapidly than $|x|$ as $x \to x_0$, i.e.

$$I := \int_a^b dx \, \frac{1}{x - x_0} \phi(x) \tag{3.11}$$

where the interval $[a, b]$ includes the divergent point x_0.

Hadamard's procedure [16] to make the above integral finite is to make a constant subtraction equal to the divergent function multiplied by ϕ evaluated at the point of divergence, i.e

$$\text{finite}[I] = \int_a^b dx \, \frac{1}{x - x_0} [\phi(x) - \phi(x_0)] \tag{3.12}$$

We can show that this subtraction is sufficient to remove the divergence by expanding the ϕ terms about the point of divergence,

$$\begin{aligned} \text{finite}[I] &= \int_a^b dx \, \frac{1}{x - x_0} \left[\phi(x_0) - \phi(x_0) + (x - x_0)\phi'(x_0) + \mathcal{O}((x - x_0)^2)\right] \\ &= \int_a^b dx \, \left[\phi'(x_0) + \mathcal{O}(x - x_0)\right] \end{aligned}$$

the integral is now convergent[1]. The plus distribution, $\frac{1}{(1-x)_+}$, is a well known example of just such a regularization of an otherwise divergent function, which is

[1] Should the power of the divergent function be more severe then we can always make further subtractions provided that the test function ϕ is sufficiently differentiable. For example in the following case we have raised the power of the denominator to some arbitrary n,

$$I := \int_a^b dx \, \frac{1}{(x - x_0)^n} \phi(x) \tag{3.13}$$

defined as,

$$\int_0^1 dx \, \frac{\phi(x)}{(1-x)_+} := \int_0^1 dx \, \frac{\phi(x) - \phi(1)}{1-x} \tag{3.16}$$

where ϕ is the test function.

3.3.1 Loop integrals

Returning to physics we shall now combine Lagrange polynomials with distribution theory to remove the soft divergences from virtual Feynman graphs. We begin with an arbitrary 1 loop integrand with n propagators,

$$I_n = \prod_{i=1}^{n} \frac{i}{a_i + i\epsilon}, \tag{3.17}$$

where $a_i = (k + p_i)^2 - m_i^2$, k is the free loop momentum to be integrated over and p_i are the various external momenta. By (3.10) this is equal to,

$$I_n = \sum_{i=1}^{n} \frac{1}{a_i + i\epsilon} \prod_{j=1,\, j\neq i}^{n} \frac{1}{a_j - a_i} \tag{3.18}$$

Because each inverse propagator has a common loop momentum term, k^2, a_j evaluated at the point at which a_i becomes on-shell is simply equal to $a_j - a_i$[1]. (3.10) is simply the statement that **a 1 loop Feynman integral is equal to the sum of Hadamard subtractions for divergences associated with each propagator**.

In this case it is necessary to subtract the first n terms of the expansion of ϕ about x_0.

$$\text{finite}[I] = \int_a^b dx \, \frac{1}{(x-x_0)^n} \left[\phi(x) - \sum_{i=0}^{n-1} \phi^{(i)}(x_0) \frac{(x-x_0)^i}{i!} \right] \tag{3.14}$$

such that we are left with,

$$\int_a^b dx \left[\frac{\phi^{(n)}(x_0)}{n!} + \mathcal{O}(x-x_0)^{n+1} \right] \tag{3.15}$$

[1]We have assumed that all propagators have the same ϵ so that they cancel when the difference of two propagator denominators is taken. This assumption is in all probability illegitimate for reasons that will be discussed in § 3.8. We shall stick to this notation for now as it is considerably simpler than giving every propagator its own ϵ.

From now on we shall refer to a Hadamard subtraction made for a massive propagator simply as a 'massive subtraction' and likewise for a massless propagator. In § 3.5 we show that the massless subtractions are IR divergent whilst the massive ones are finite in the soft limit.

We choose to define the convergent part of an arbitrary loop integrand as being equal to the sum of all massive (soft convergent) subtractions, i.e. it is equal to the full integrand minus the massless subtractions. The major benefit of this definition is that it allows us to write the difference of the original integrand and its subtraction terms as a sum of terms each of which is individually finite such that they can be evaluated in four dimensions numerically.

3.4 Cutting Equations

The soft subtractions for the virtual graphs must be equal, up to an opposite sign, to the subtractions for the real graphs in order for the full cross section to be preserved. For every virtual integrand there is a conjugate one so in fact the subtraction term that must be added back into the real graph is twice the real part of the virtual subtraction term. Taking into account all of the factors of i that we have otherwise omitted from the calculations this amounts to taking twice the imaginary part of the integrand in our notation.

We can extract the imaginary part of (3.18) as follows,

$$2\Im\left(\prod_{i=1}^{n}\frac{1}{a_i+i\epsilon}\right)=\sum_{i=1}^{n}\left(\frac{1}{a_i+i\epsilon}-\frac{1}{a_i-i\epsilon}\right)\prod_{j\neq i}^{n}\frac{1}{a_j-a_i} \tag{3.19}$$

If we now take the limit $\epsilon \to 0$ then we can replace the massless propagator with its on-shell delta representation,

$$2\Im\left(I_n\right)=\sum_{i=1}^{n}2\pi\delta(a_i)\prod_{j\neq i}^{n}\frac{1}{a_j-a_i} \tag{3.20}$$

This form of the massless subtraction is beginning to look very much like a term which could be added to the corresponding real correction graph because the massless propagator is now in its phase space form, this implies that all instances

of its argument a_i must be identically zero so we can further simplify the expression above by dropping a_i from all other propagators (3.21).

$$2\Im\left(I_n\right) = \sum_{i=1}^{n} 2\pi\delta(a_i) \prod_{j\neq i}^{n} \frac{1}{a_j} \tag{3.21}$$

This tells us that the imaginary part of the graph is equal to the sum of all possible single particle cuts.

3.5 Proof of infrared finiteness

We can prove the finiteness of the sum of the massive subtractions by noting that all massless propagators disappear when we factorize it. Explicitly what we wish to show is that if we take an arbitrary integrand I_n with m massive and $n-m$ massless propagators,

$$I_n = \prod_{i=1}^{n} \frac{1}{a_i + i\epsilon}, \tag{3.22}$$

Lagrange decompose it and then re-sum all of the massive subtractions, then the resulting expression has the following form[1]:

$$\sum_{i=1}^{m} \frac{1}{a_i + i\epsilon} \prod_{j\neq i}^{n} \frac{1}{a_j - a_i} = \mathbf{N} \prod_{i=1}^{m} Q_m(a_i) \tag{3.24}$$

where $\mathbf{N}$ is some polynomial composed of various a_i's and

$$Q_m(a_i) = \frac{1}{a_i} \prod_{j=m+1}^{n} \frac{1}{a_j - a_i}. \tag{3.25}$$

[1]In fact any partial resummation of the terms in the Lagrange decomposition series must have an equivalent form. In this case where we are re-summing the Lagrange decomposition terms into two sets, massive and massless, the $a_j - a_i$ part is identical in both cases, i.e. the expression for the sum of massless terms is

$$\sum_{i=m+1}^{n} \frac{1}{a_i + i\epsilon} \prod_{j\neq i}^{n} \frac{1}{a_i - a_j} = \mathbf{N}' \prod_{i=m+1}^{n} Q_{n-m}(a_i) \tag{3.23}$$

.

This result is proved in appendix B. As $i \leq m$ the a_i terms are massive and cannot become singular in the soft limit, and as $j > m$ the difference $a_j - a_i$ must also contain a mass therefore there are no massless terms in the denominator.

It has been proved [25] that Feynman graphs with all massive propagators do not contain infrared singularities. This proof assumes that the inverse propagator has a quadratic form whereas we consider those which necessarily do not. However the soft behavior of the non quadratic propagators cannot be any more severe than the quadratic ones. We hope, but have not proved, that this line of reasoning will allow us to bound the Lagrange decomposition finite integrals by the result obtained for the full quadratic propagators.

3.6 Example calculations

Sector decomposition [1] has been used successfully used for practical calculations can we use the Lagrange interpolation method as well? In this section we shall put (3.10) to use and explicitly remove the soft divergences from 3 example loop integrals.

3.6.1 A triangle graph with one massless propagator

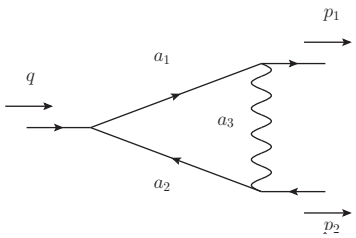

Figure 3.2: Triangle graph with one massless line.

The integrand for fig. 3.2 is written schematically as $\prod_{i=1}^{3} \frac{1}{a_i + i\epsilon}$ and by (3.10) this is equal to,

$$I_3 = \frac{1}{a_1 + i\epsilon} \frac{1}{a_2 - a_1} \frac{1}{a_3 - a_1} + \frac{1}{a_1 - a_2} \frac{1}{a_2 + i\epsilon} \frac{1}{a_3 - a_2} + \frac{1}{a_1 - a_3} \frac{1}{a_2 - a_3} \frac{1}{a_3 + i\epsilon}.$$

Only the last of the three terms on the r.h.s. is infrared divergent, this has nearly the form of the usual eikonal approximation (except for the missing $i\epsilon$ in the massive propagators),

$$\frac{1}{a_1 - a_3}\frac{1}{a_1 - a_3}\frac{1}{a_3 + i\epsilon} = \frac{1}{2k \cdot p_1}\frac{1}{-2k \cdot p_2}\frac{1}{k^2 + i\epsilon} \tag{3.26}$$

It is well known that the eikonal approximation captures the full soft behavior of the integrand so in order to make the full integrand finite we drop this term from the sum.

$$\text{finite}[I_3] = \sum_{i\neq 3}^{3} \frac{1}{a_i + i\epsilon} \prod_{j\neq i}^{3} \frac{1}{a_j - a_i} \tag{3.27}$$

Although the massive subtraction terms contain a common massless propagator $\frac{1}{a_1 - a_2}$ this will disappear when we add the two terms together,

$$\text{finite}[I_3] = \frac{a_1 + a_2 - a_3}{(a_1 + i\epsilon)(a_3 - a_1)(a_2 + i\epsilon)(a_3 - a_2)}. \tag{3.28}$$

The expression above now has the form of (3.24), as it contains no massless terms in the denominator it must be finite in the soft limit.

However, the massless subtraction is not only infrared divergent but UV divergent as well, which implies that the rest of the integrand is also UV divergent. We can fix this by multiplying the original integrand by a suitable partition of unity which separates infrared and UV behavior such as $1 = \frac{a_3}{a_3 - \lambda} - \frac{\lambda}{a_3 - \lambda}$.

Our strategy is to split up the integrand into a manifestly infrared finite piece and another piece with the same infrared behavior as the original but with an extra UV protecting term, i.e.

$$\begin{aligned} I_3 &= \frac{1}{a_1 + i\epsilon}\frac{1}{a_2 + i\epsilon}\frac{1}{a_3 + i\epsilon}\left(\frac{a_3}{a_3 - \lambda} - \frac{\lambda}{a_3 - \lambda}\right) \\ &= \frac{1}{a_1 + i\epsilon}\frac{1}{a_2 + i\epsilon}\frac{1}{a_3 - \lambda + i\epsilon} \\ &\quad - \frac{1}{a_1 + i\epsilon}\frac{1}{a_2 + i\epsilon}\frac{1}{a_3 + i\epsilon}\frac{\lambda}{a_3 - \lambda + i\epsilon} \end{aligned}$$

It is now safe to proceed as before with the infrared on the last line of the

expression above.

$$\begin{aligned}\text{finite}[I_3] = &\frac{1}{a_1+i\epsilon}\frac{1}{a_2+i\epsilon}\frac{1}{a_3-\lambda+i\epsilon} \\ &- \frac{a_1+a_2-a_3}{(a_1+i\epsilon)(a_3-a_1)(a_2+i\epsilon)(a_3-a_2)}\frac{\lambda}{a_3-\lambda+i\epsilon}\end{aligned} \tag{3.29}$$

3.6.2 A box graph with two massless propagators.

This second example is simpler in so much that there is no need to provide any additional UV protection. In this graph there are two massless propagators which will each require a subtraction. The integrand for fig. 3.3 is,

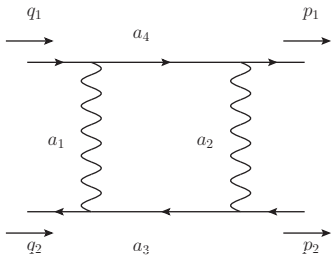

Figure 3.3: Box graph with two massless lines.

$$I_4 = \prod_{i=1}^{4}\frac{1}{a_i+i\epsilon} \tag{3.30}$$

We begin as before by using (3.10),

$$\begin{aligned}I_4 = &\frac{1}{a_1+i\epsilon}\frac{1}{a_2-a_1}\frac{1}{a_3-a_1}\frac{1}{a_4-a_1} + \frac{1}{a_1-a_2}\frac{1}{a_2+i\epsilon}\frac{1}{a_3-a_2}\frac{1}{a_4-a_2} \\ &+ \frac{1}{a_1-a_3}\frac{1}{a_2-a_3}\frac{1}{a_3+i\epsilon}\frac{1}{a_4-a_3} + \frac{1}{a_1-a_4}\frac{1}{a_2-a_4}\frac{1}{a_3-a_4}\frac{1}{a_4+i\epsilon}\end{aligned} \tag{3.31}$$

and dropping the terms that are infrared divergent we have,

$$\text{finite}[I_4] = \sum_{i\notin\{1,2\}}^{4}\frac{1}{a_i+i\epsilon}\prod_{j\neq i}^{4}\frac{1}{a_i-a_j} \tag{3.32}$$

If we can combine the massless and massive subtractions into two expressions,

$$I_4 = \frac{a_1^2 + a_1\,a_2 + a_2^2 - (a_1 + a_2)\,(a_3 + a_4) + a_3\,a_4}{(a_1 + i\epsilon)\,(a_3 - a_1)\,(a_4 - a_1)\,(a_2 + i\epsilon)\,(a_3 - a_2)\,(a_4 - a_2)} + \frac{a_3^2 + a_3\,a_4 + a_4^2 - (a_3 + a_4)\,(a_1 + a_2) + a_1\,a_2}{(a_3 + i\epsilon)\,(a_1 - a_3)\,(a_2 - a_3)\,(a_4 + i\epsilon)\,(a_1 - a_4)\,(a_2 - a_4)}. \tag{3.33}$$

Again we note that in the massive sum (bottom line) all the massless propagators have disappeared leaving us with a completely massive denominator, whilst in the massless sum (top line) there is a corresponding completely massless denominator, as such the finite part of the box graph is simply,

$$\text{finite}[I_4] = \frac{a_3^2 + a_3\,a_4 + a_4^2 - (a_3 + a_4)\,(a_1 + a_2) + a_1\,a_2}{(a_3 + i\epsilon)\,(a_1 - a_3)\,(a_2 - a_3)\,(a_4 + i\epsilon)\,(a_1 - a_4)\,(a_2 - a_4)}. \tag{3.34}$$

3.6.3 A double box graph with three massless propagators.

Now we turn our attention to a two loop example. Like the single box there is no need to employ a UV regulator.

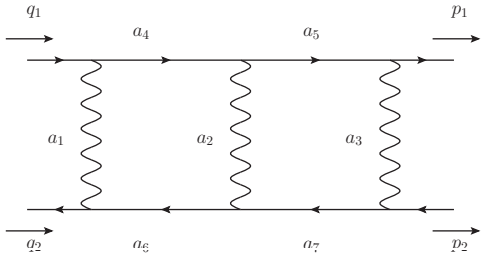

Figure 3.4: Double box with 3 massless lines.

Despite the fact that there are now multiple overlapping infrared divergences we can blithely follow the same procedure as before using (3.18) to expand the integrand but drop the terms $i \in \{1, 2, 3\}$ to remove the infrared divergences,

$$\text{finite}[I_7] = \sum_{i \notin \{1,2,3\}}^{7} \frac{1}{a_i + i\epsilon} \prod_{j \neq i}^{7} \frac{1}{a_j - a_i}, \tag{3.35}$$

and that is it. No special consideration is taken for the fact that this is a multi-loop graph. Again we can re-sum the massive / massless subtractions and observe the cancellation of all massless propagators in the massive sum and vice versa [1]. However the numerator in the re-summed subtractions now has a very complicated form, fully expanded it contains over a thousand terms. Although this can be simplified considerably no closed form solution for an arbitrary numerator has been found.

3.7 α representation

There already exists a well known method to decompose Feynman integrals into pieces to disentangle its divergences called Sector Decomposition first uesd to disentangle UV divergences [19] and later developed to isolate the infrared divergences [5]. In this section we shall show that there is an informal but illuminating link between the two methods.

Let us revert to the partition of unity (3.9). Each $\frac{A_j}{A_j - A_i}$ acts as a smooth step function that imposes the condition that A_i tends to zero faster than A_j. I.e. for $|A_i| > |A_j|$ and $A_j \to 0$ we have,

$$\frac{A_j}{A_j - A_i} \to 0 \tag{3.36}$$

while for $|A_j| > |A_i|$ and $A_i \to 0$ we have,

$$\frac{A_j}{A_j - A_i} \to 1 \tag{3.37}$$

We can now interpret (3.9) as the sum of over all i where A_i is softer than any other propagator. This is closely related in spirit to the method of Sector Decomposition. Sector Decomposition explicitly orders the α (Feynman) parameters in

[1] This factorization can be achieved in the order of a few seconds in a symbolical algebra program such as Maple or Mathematica.

magnitude by step functions.

$$\prod_{i=1}^{n}\frac{1}{A_i}=\int_0^1 d\alpha_i\frac{\delta(1-\sum\alpha_i)}{[A_i\cdot\alpha_i]^n}\theta(\alpha_1>\alpha_2>\cdots>\alpha_n)+\text{permutations} \tag{3.38}$$

where $\theta(\alpha_1>\alpha_2>\cdots>\alpha_n)=\theta(\alpha_1-\alpha_2)\theta(\alpha_2-\alpha_3)\cdots\theta(\alpha_{n-1}-\alpha_n)$. It has been shown [20] that Sector Decomposition can be mapped to momentum space where it has the following form,

$$\prod_{i=1}^{n}\frac{1}{A_i}=\prod_{i=1}^{n}\frac{1}{\sum_{j=1}^{i}A_j}+\text{permutations} \tag{3.39}$$

Though this is not the same procedure as the Lagrange decomposition method it is nevertheless instructive to complete the circle and investigate exactly what form (3.10) takes in α space. We begin by using the partition of unity recursively to order all propagators.

$$1=\sum_{i_0=1}^{n}\left(\sum_{i_1\neq i_0}^{n}\frac{A_{i_1}}{A_{i_1}-A_{i_0}}\left(\sum_{i_2\neq i_1}^{n}\frac{A_{i_2}}{A_{i_2}-A_{i_1}}\left(\cdots\sum_{i_n\neq i_{n-1}}^{n}\frac{A_{i_n}}{A_{i_n}-A_{i_{n-1}}}\right)\right)\right) \tag{3.40}$$

which can be written as,

$$1=\prod_{j=1}^{n}\sum_{i_j\neq i_{j-1}}^{n}\frac{A_{i_j}}{A_{i_j}-A_{i_{j-1}}}, \tag{3.41}$$

where $A_{i_0}:=0$. Multiplying both sides by $\prod_{i=1}^{n}\frac{1}{A_i}$ again we have,

$$\prod_{i=1}^{n}\frac{1}{A_i}=\prod_{i=1}^{n}\frac{1}{A_i-A_{i-1}}+\text{permutations.} \tag{3.42}$$

After Feynman parametrization we have,

$$\prod_{i=1}^{n}\frac{1}{A_i}=\int_0^1 d\alpha_1\cdots d\alpha_n\frac{\delta(1-\sum\alpha_i)}{[A_i(\alpha_1-\alpha_2)+A_2(\alpha_2-\alpha_3)\cdots A_n\alpha_n]^n}+\text{permutations} \tag{3.43}$$

We now change variables to $\beta_i = \alpha_i - \alpha_{i+1}$, $\beta_n = \alpha_n$ (this conveniently has a Jacobian of 1) which gives,

$$\prod_{i=1}^{n} \frac{1}{A_i} = \int_{-1}^{1} d\beta_1 \dots d\beta_n \frac{\delta(1 - \sum i \cdot \beta_i)}{[A_i \cdot \beta_i]^n} + \text{permutations} \tag{3.44}$$

As expected we see that the delta function $\delta(1-\beta_1-2\beta_2-3\beta_3-\cdots n\beta_n)$, weights the β parameters, and hence the propagators, in a manner similar to that of Sector Decomposition.

3.8 Practicalities of numerical evaluation

Implicit in all analysis done so far is the assumption that all $i\epsilon$ regulators are the same, this has allowed us to remove the ϵ terms from all but the first term in the Lagrange decomposition. In reality this cannot be strictly true. It could be argued that as all soft divergences have been explicitly removed from the integrand the ϵ plays no role in regularizing singularities that no longer exist. Certainly we cannot sensibly use an infinitesimally small parameter in any numerical procedure so we may as well drop the ϵ at the first instance that it becomes unnecessary.

Of course soft divergences are not the only singularities in the game. Up to this point we have used the terms divergence, on-shell, and singularity interchangeably, but in fact although a propagator being on-shell will give rise to singularity it is not necessarily a divergent one A non divergent singularity will not contribute to the soft behavior of the integrand but it will require an $i\epsilon$ to regulate it. In chapter 4 we shall explore these non divergent singularities extensively and shall pay particular attention to how we can correctly remove the $i\epsilon$ terms to allow a numerical evaluation.[1]

[1] If we do attempt to evaluate the Feynman parameter integrals for massive subtractions naively without any ϵ then what we get from the Monte Carlo is just noise typical of an attempt to evaluate a completely massive graph by Monte Carlo without paying due attention to its threshold behavior fig. 4.2.

Chapter 4

Numerical computation of threshold singularities

In this chapter we present a new method to perform the numerical integration of threshold singularities. Rather than perform the usual 'contour deformation' approach [26] we shall identify the troublesome poles for a given external kinematic configuration and move them within the complex plane such that the integration contour does not cross any branch cuts. The principle appeal of this method is its simplicity.

4.1 Introduction

Threshold singularities occur when two or more virtual propagators become on-shell simultaneously. Such singularities can be readily identified by use of the cutting equations [11] whilst the Coleman-Norton theorem [10] shows us how to interpret thresholdF1 singularities as classically allowed processes. Threshold singularities are in fact 'integrable' which suggests that with enough computing power they should be straightforward to evaluate numerically. However a simple example reveals the fallacy of this logic especially if we attempt to perform these integrals by Monte Carlo,

$$\lim_{\epsilon \to 0} \int_{-1}^{1} dx \, \frac{1}{x + i\epsilon} = i\pi. \tag{4.1}$$

We cannot easily implement the integration above in a Monte Carlo routine because it is not at all clear how to represent the infinitesimal quantity ϵ. If we simply ignore ϵ by setting it to zero then 1000 points in the GSL Vegas routine gives the answer $-1.982508(1.293820)$. This example illustrates an important point: we know a priori that the probability amplitude will be complex valued. A naive Monte Carlo routine will evaluate the real part with an infinite variance and will never produce an answer for the imaginary part of such a complex function. Integrable singularities are ubiquitous in perturbative calculations with massive virtual propagators.

4.1.1 Calculation preliminaries

For simplicity all the graphs we shall study in this chapter are restricted to scalar particles with all masses equal. The virtual propagators are denoted by $\frac{1}{a_i+i\epsilon}$ with a corresponding Feynman parameter x_i where $i = 1, 2, ...$ All external particles are on-shell and their momenta are denoted as, $p_1, ..., p_4$, which are all incoming and the usual Mandelstam convention is used, $s = (p_1 + p_2)^2$, $t = (p_1 + p_4)^2$ and $u = (p_1 + p_3)^2$.

For example the triangle graph, fig. 4.1, has the following integrand (4.2).

$$I_3(s) = \int d^4k \, \frac{1}{a_1 + i\epsilon} \frac{1}{a_2 + i\epsilon} \frac{1}{a_3 + i\epsilon} \tag{4.2}$$

Before we perform Feynman parametrization,

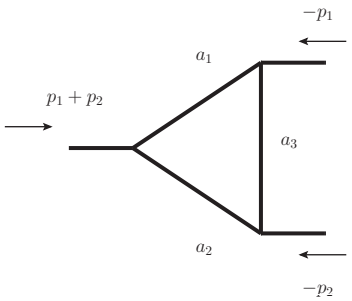

Figure 4.1: Scalar massive triangle graph, $I_3(s)$.

$$\frac{1}{A\,B} = \int_0^1 dx\, \frac{1}{[A\,x + B\,(1-x)]^2} \tag{4.3}$$

we should remember that the identity above only holds for $\Re(A) > 0$ and $\Re(B) > 0$, later we shall see that these conditions are not always satisfied and that this will cause integral to diverge.

Performing the virtual k integral analytically we have (4.4).

$$I_3(s) = \int_0^1 dx_1\, dx_2\, dx_3\, \frac{\delta(1 - x_1 - x_2 - x_3)}{[s\,x_1\,x_2 + m^2\,(x_1 + x_2)\,x_3 - m^2 + i\epsilon]} \tag{4.4}$$

A naive Monte Carlo integration over the Feynman parameters produces the graph in fig. 4.2. The numerical procedure works well, indeed correctly, up to

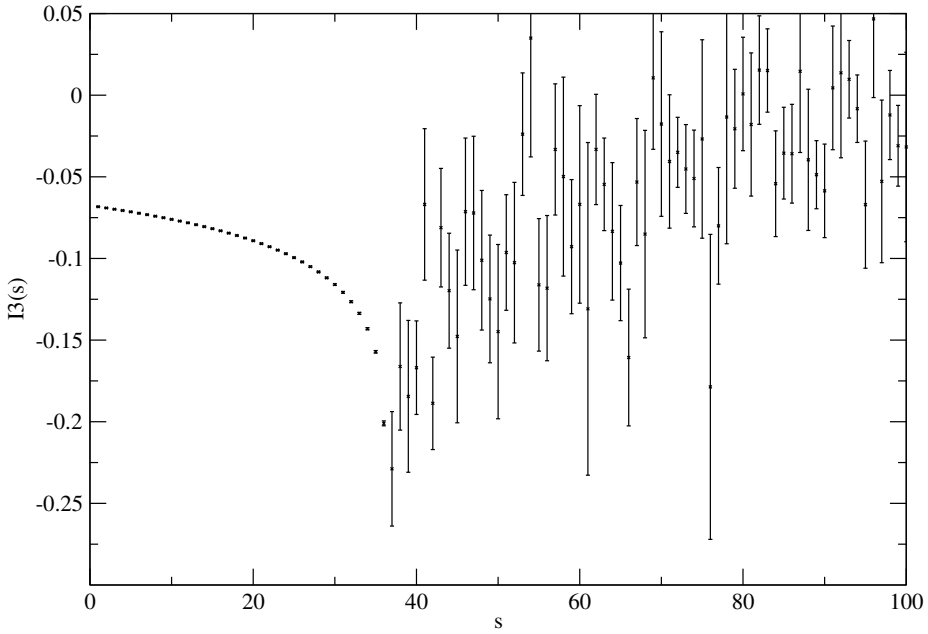

Figure 4.2: The result of a naive Monte Carlo integration of (4.4). Note that the integration routine finds the correct result up to $s = 4m^2$ which is the point where the intermediate virtual particles can simultaneously become real.

the point $s = 4m^2$, and thereafter it fails, why? It is well known [28] that for the cut in s channel the triangle graph has the same threshold structure as the reduced graph in fig. 4.3, In terms of Feynman parameters fig. 4.1 corresponds to

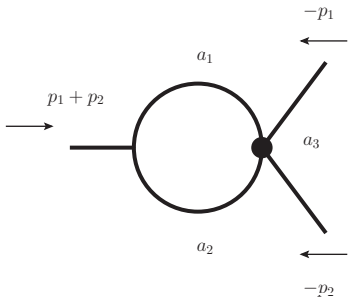

Figure 4.3: The reduced graph of fig. 4.1 for the s-channel cut which corresponds to Feynman parameters $\{x_i\} = \{2^{-1}, 2^{-1}, 0\}$

.

$\{x_i\} = \{x_1, x_2, 0\}$ and hence the integrand is reduced to,

$$I_3(s) \Rightarrow \int_0^1 dx_1 \, \frac{1}{[s\, x_1\, (1 - x_1) - m^2 + i\epsilon]}. \tag{4.5}$$

The denominator is now a quadratic in x_1 (x_2 is trivially removed by the delta function) whose discriminant at $\epsilon = 0$ is $\sqrt{s^2 - 4\, s\, m^2}$. We note that for $s < 4m^2$ the roots are both imaginary, whilst for $s > 4m^2$ the roots are real and thus are on the integration contour. It is at this point that there is sufficient incoming energy for both propagators a_1 and a_2 to become on shell simultaneously. Substituting the position of the pole $s = 4\, m^2$ into (4.5) we see that the Feynman parameters for the pole at $x_1 = x_2 = 1/2$.[1]

$$I_3(s) \Rightarrow \frac{1}{[s/4 - m^2 + i\epsilon]}. \tag{4.6}$$

More generally the cutting equations tells us that the integrand will have a branch cut when any intermediate states become on shell.

In the next section, § 4.2 we shall introduce a procedure to move the trou-

[1]It is tempting to try and overcome this issue by formulating a Hadamard style subtraction about the point where more than one propagator becomes on shell but in practice there are good reasons why we have chosen not to. Firstly it is all but impossible to do this covariantly. Furthermore unlike the infrared scenario we do not wish to simply remove the singularity, any subtraction that we could make would have to be evaluated in full at some point later anyway. Lastly there is not much point in performing any subtraction that does not separate the integral into its real and imaginary parts, and in any case we have found no such procedure.

blesome poles away from the contour such that the integrals can be performed numerically, and give a couple of simple one loop examples. In § 4.3 we introduce a further trick ostensibly to extend this method to a graph where it should fail and we note that this also naturally regularizes ultra-violet divergences.

4.2 The method - 'Pole Rotation'

Our procedure is simple: we pick the kinematic channel in which we wish to evaluate the graph, we then use the cutting equations to identify which propagators could become on-shell and multiply their numerators and denominators by i. We refer to this as 'rotation', as although it only involves multiplication by 1, it introduces a complex phase between the denominators of the propagators. We shall see how Feynman parametrization makes the complex phase i non trivial and facilitates the numerical computation of the graph.

It might appear that this procedure can do no wrong as, after all, it only involves multiplication by 1 and that our instance that it is the cut propagators that should be rotated relative to the un-cut ones is unnecessary. Why not rotate any random selection of propagators? In fact there is the possibility of introducing spurious numerical instabilities which we examine in the next section.

4.2.1 Triangle example

The introduction of i into the denominator of the loop integrand will alter the position of its poles in the complex plane and, unless we are careful, render the usual Wick rotation used to perform the virtual integral invalid. Before we proceed we must determine exactly where these poles are so that we can move them in a manner consistent with the Feynman $i\epsilon$ prescription. In all the graphs considered here there are no infrared poles, and for the moment we shall not consider ultraviolet poles either, therefore all poles must originate from the thresholds themselves. For any given channel the cutting equations tell us exactly which propagators contribute to these poles, and this can be translated into x space. We have already seen in the triangle example there is only one pole located

at $x_i = \{2^{-1}, 2^{-1}, 0\}$. Multiplying the denominator, a_3, by i we have (4.7).

$$I_3(s) = \int d^4k \, \frac{1}{a_1} \frac{1}{a_2} \frac{i}{i\,[a_3 + i\epsilon]}, \tag{4.7}$$

This will not affect the pole structure of the triangle integrand in the s-channel because a_3 is simply not part of it. Alternatively we could multiply the propagators that contribute to the pole $\{a_1, a_2\}$ by i, (4.8),

$$I_3(s) = \int d^4k \, \frac{i}{i\,[a_1 + i\epsilon]} \frac{i}{i\,[a_2 + ie]} \frac{1}{a_3 + i\epsilon}, \tag{4.8}$$

this is consistent with the $i\epsilon$ prescription so long as we rotate all the pole propagators by the same factor so causality is unaffected. Either way we are rotating the pole part of the graph with respect to the rest of it, as such the pole structure is unaffected and the original integral can be recovered by multiplying by i raised to the power of the number of cut propagators.

In practice we use a sequential pairwise Feynman parametrization, $\{y_i\}$, which automatically removes the delta function such that the integration is over an $n-1$ hypercube. This can be achieved by a change of variables $x_1 = y_1\, y_2$, $x_2 = \bar{y}_1\, y_2$ and $x_3 = \bar{y}_3$ where $\bar{y}_i = 1 - y_i$. Performing the virtual k integral again for (4.7) with the $\{y_i\}$ parameters we now get (4.9).

$$I_3(s) = -i \int_0^1 dy_1\, dy_2 \, \frac{y_2}{y_2 + i\bar{y}_2} \frac{1}{[s\, y_1\, \bar{y}_1 - m^2]\, y_2^2 - i\, m^2\, \bar{y}_2\, (y_2 + i\, \bar{y}_2) + i\epsilon} \tag{4.9}$$

The pole is now located at $\{y_i\} = \{2^{-1}, 2^{-1}, 1\}$. This expression can be broken up into its real and imaginary parts which can be evaluated separately using the Monte Carlo Vegas routine, though in practice it is computationally cheaper to perform the integration in the complex plane and then separate the result fig. 4.4. It is important to note that we can now set $\epsilon = 0$ in the Monte Carlo routine because there is now a non-negligible term in the denominator which will dominate any infinitesimal $i\epsilon$.

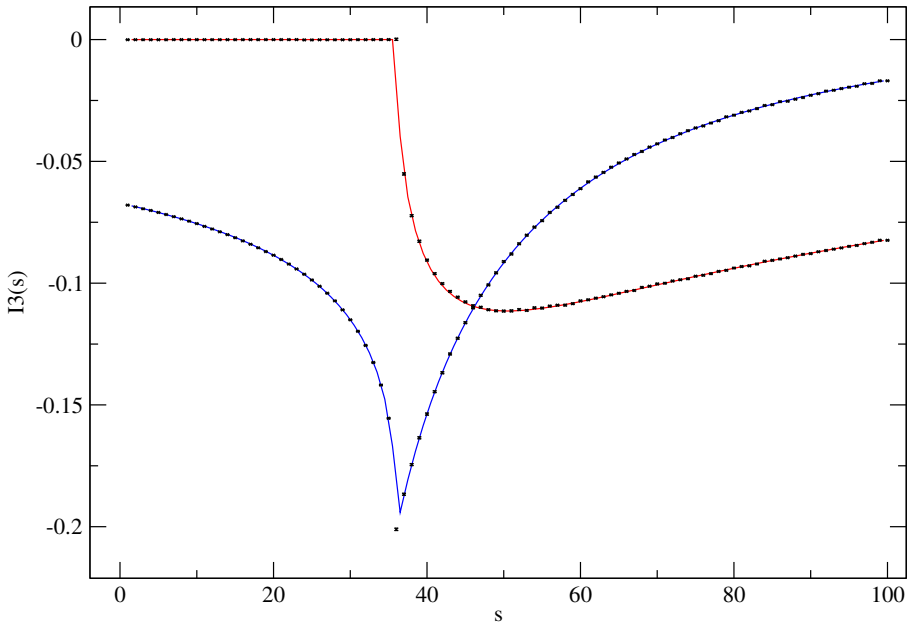

Figure 4.4: The black crosses are the result of the complex Monte Carlo integration of (4.9) for $m = 3$. The blue line is the exact real part and the red line is the exact imaginary part of the amplitude result obtained from QCDLoops [13].

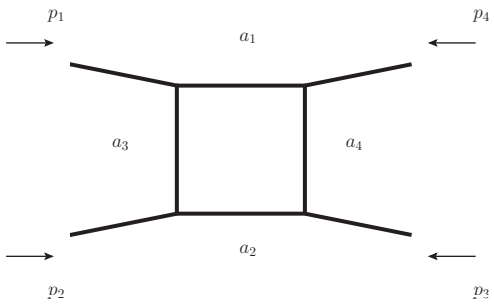

Figure 4.5: The box graph corresponding to (4.10), $I_4(s)$

4.2.2 Box graph

We can apply exactly the same procedure to the massive box integral fig. 4.5, (4.10).

$$I_4(s,t) = \int d^4k \, \frac{1}{a_1 + i\epsilon} \frac{1}{a_2 + i\epsilon} \frac{1}{a_2 + i\epsilon} \frac{1}{a_4 + i\epsilon} \tag{4.10}$$

which has the following parametric form,

$$I_4(s,t) = \int d^4k \int_0^1 \frac{dx_1\, dx_2\, dx_3\, dx_4 \quad \delta(1-x_1-x_2-x_3-x_4)}{[k^2 + s\, x_1x_2 + m^2\,(x_1+x_2)\,(x_3+x_4) + t\, x_3x_4 - m^2 + i\epsilon]^2}. \tag{4.11}$$

This time there are two ways of cutting the graph: the s-channel cut which has the reduced graph fig. 4.6 that corresponds to Feynman parameters $x_i = \{2^{-1}, 2^{-1}, 0, 0\}$; and the t-channel cut which has the reduced graph fig. 4.7 which corresponds to Feynman parameters $x_i = \{0, 0, 2^{-1}, 2^{-1}\}$. There is a pole in both the t and s-channel cut but they are disjoint in momentum space and so we need not worry about any overlap. Applying what we have learnt from the triangle

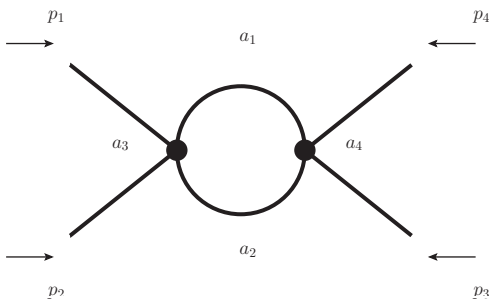

Figure 4.6: The reduced graph of fig. 4.5 for the s-channel cut which corresponds to Feynman parameters $x_i = \{2^{-1}, 2^{-1}, 0, 0\}$.

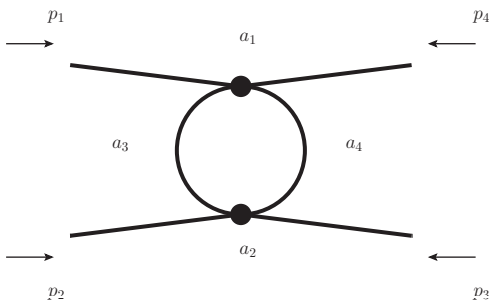

Figure 4.7: The reduced graph of fig. 4.5 for the t-channel cut which corresponds to Feynman parameters $x_i = \{0, 0, 2^{-1}, 2^{-1}\}$.

we see that we can deal with the s-channel pole by rotating the propagators that

contribute to it $\{a_1, a_2\}$,

$$I_4(s,t) = \int d^4k \, \frac{i}{i\,[a_1 + i\epsilon]} \frac{i}{i\,[a_2 + i\epsilon]} \frac{1}{a_2 + i\epsilon} \frac{1}{a_4 + i\epsilon} \tag{4.12}$$

Alternatively we could also rotate the rest of the graph with respect to the cut propagators in the t-channel (4.13).

$$I_4(s,t) = \int d^4k \, \frac{1}{a_1 + i\epsilon} \frac{1}{a_2 + i\epsilon} \frac{i}{i\,[a_3 + i\epsilon]} \frac{i}{i\,[a_3 + i\epsilon]} \tag{4.13}$$

The s - t crossing symmetry in this graph means that any procedure that works for the s-channel will also work for the t-channel. In fact both rotations are equivalent as they both rotate the same pairs of propagators with respect to each other. Suppose we pick the s-channel rotation and use the following change of variables $x_1 = y_1\, y_3$, $x_2 = \bar{y}_1\, y_3$, $x_3 = y_2\, \bar{y}_3$ and $x_4 = \bar{y}_2\, \bar{y}_3$ then we get the following integrand,

$$I_4(s,t) = \int_0^1 dy_1\, dy_2\, dy_3 \, \frac{-4\, y_3\, \bar{y}_3}{[[s\, y_1\, \bar{y}_1 - m^2]\, y_3^2 - i\, m^2\, y_3\, \bar{y}_3 - [t\, y_2\, \bar{y}_2 - \, m^2]\, \bar{y}_3^2 + i\epsilon]^2}. \tag{4.14}$$

Performing the integral numerically produces the graph in fig. 4.8.

4.3 Bubble graph

The bubble graph fig. 4.9, (4.15) has the following integrand,

$$I_2(s) = \int d^4k \, \frac{1}{a_1 + i\epsilon} \frac{1}{a_2 + i\epsilon}. \tag{4.15}$$

This graph is UV divergent and needs to be renormalised. We choose to use the BPHZ procedure which involves subtracting from $I_2(s)$ itself evaluated at $s = 0$, i.e. $I_2(s) - I_2(0)$. Although BPHZ does not require any regularization of the divergent integral in practice we cannot perform the virtual loop integral for a graph with only two propagators without the use of some sort of regulating procedure. We present what we believe to be a new regulation method. This new method involves introducing a new 'propagator' that is not part of the loop

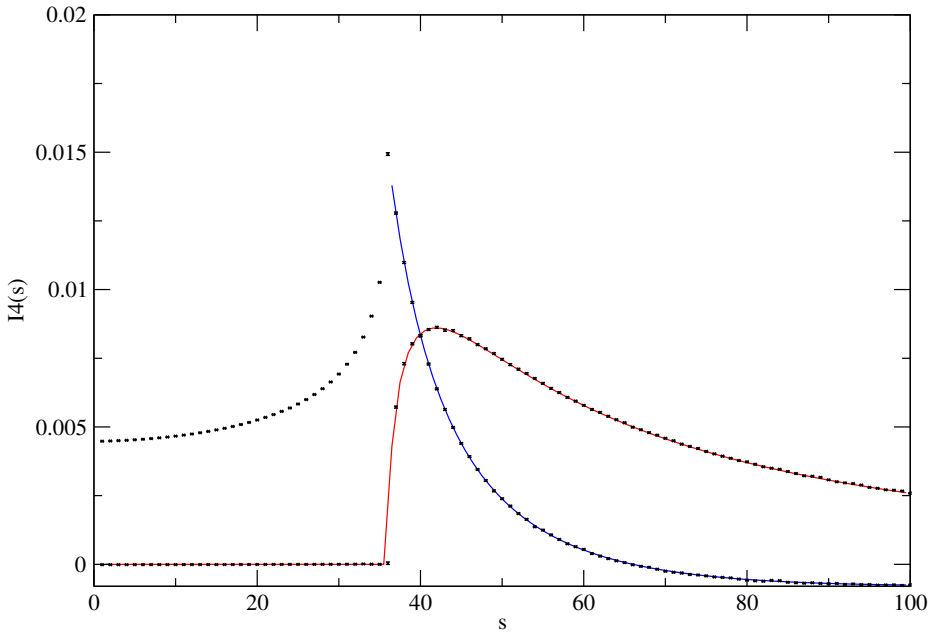

Figure 4.8: The black crosses are the result of a the complex Monte Carlo integration of (4.12) for $m = 3$. The blue line is the exact real part and the red line is the exact imaginary part of the amplitude result obtained from QCDLoops [13].

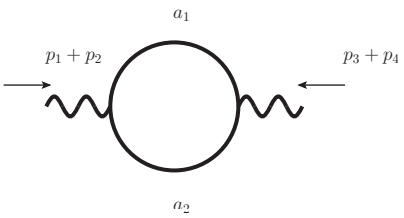

Figure 4.9: The bubble graph corresponding to (4.15), $I_2(s)$.

and does not contain the free loop momentum k, however we treat it as if it was. By adding the new dummy propagator to the graph the number of propagators is increased and virtual loop momenta can be evaluated analytically. In this example the new propagator is simply $\frac{1}{s+i\epsilon}$ which gives us (4.17).

$$\frac{I_2(s)}{s+i\epsilon} = \frac{1}{s+i\epsilon}\int d^4k \frac{1}{a_1+i\epsilon}\frac{1}{a_2+i\epsilon} \tag{4.16}$$

We can always remove this extra propagator by multiplying the result by s after renormalization. Another advantage of using this method of regulating I_2 is that

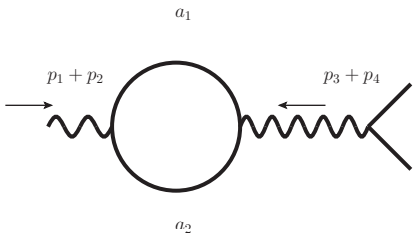

Figure 4.10: The bubble graph with an extra incoming propagator $\frac{I_2(s)}{s}$.

it gives us a non singular propagator to rotate the cut propagators with respect to:

$$\frac{I_2(s) - I_2(0)}{s + i\epsilon} = \int d^4k \frac{i}{i\,[a_1 + i\epsilon]} \left[\frac{i}{i\,[a_2 + i\epsilon]} - \frac{i}{i\,[a_1 + i\epsilon]} \right] \frac{1}{s + i\epsilon} \tag{4.17}$$

Performing the loop integral and removing the regulating propagator by multiplying by s we have the following integral,

$$I_2(s) - I_2(0) = \int_0^1 dy_1\, dy_2 \left[\frac{s}{[s\, y_1\, \bar{y}_2 - m^2]\, y_2^2 + i\, s\, y_1\, \bar{y}_2} - \frac{s}{[-m^2]\, y_2^2 + i\, s\, y_1\, \bar{y}_2} \right], \tag{4.18}$$

which evaluated by Monte Carlo give the familiar graph in fig. 4.11.

4.4 More complicated graphs.

So far we have only considered one-loop graphs, we now we turn our attention to the simplest two-loop example. The integrand for the graph in fig. 4.12 is given by

$$I_2^2(s) = \int d^4k \, \frac{1}{a_1 + i\epsilon} \frac{1}{a_2 + i\epsilon} \frac{1}{a_3 + i\epsilon} \frac{1}{a_4 + i\epsilon} \frac{1}{a_5 + i\epsilon}. \tag{4.19}$$

There are four possible threshold poles for the graph above which correspond to the reduced graphs in fig. 4.13,

Suppose we look at fig. 4.13 (a) in isolation, according to the procedure outlined in the previous sections we should rotate the cut propagators $\{a_1, a_2\}$ with respect to the others $\{a_3, a_4, a_5\}$. However applying the same rules to fig. 4.13 (b)

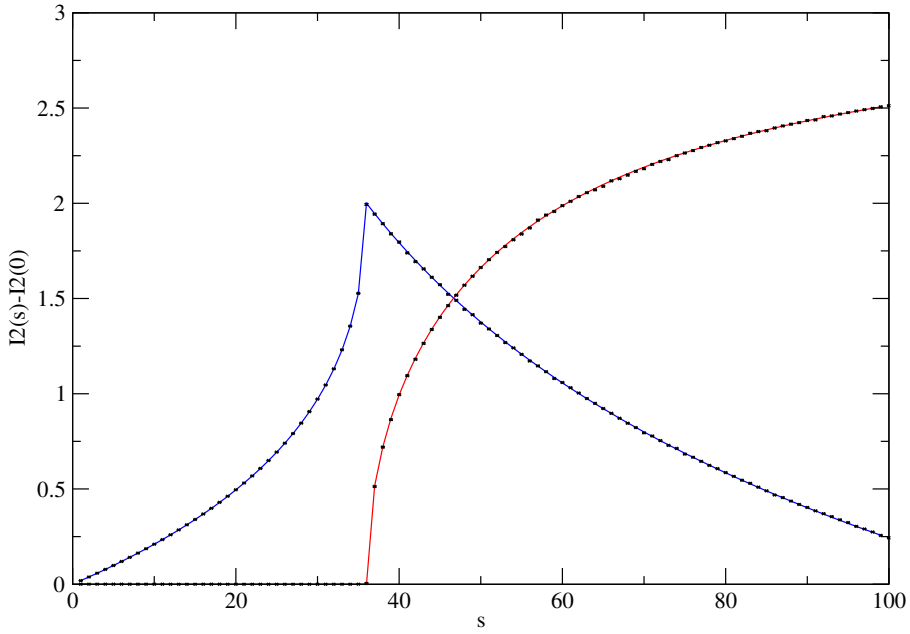

Figure 4.11: The black crosses are the result of the complex Monte Carlo integration of (4.18) for $m = 3$. The blue line is the exact real part and the red line is the exact imaginary part of the amplitude result obtained from QCDLoops [13].

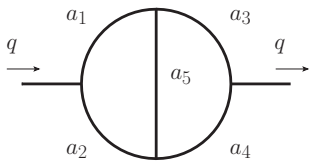

Figure 4.12: A simple two-loop graph, $I_2^2(s)$

would require rotating $\{a_2, a_3, a_5\}$ with respect to $\{a_1, a_4\}$ which is incompatible with our prescription for fig. 4.13 (a).

It should be noted that although there are overlapping thresholds in momentum space in parameter space they are quite distinct. One possible solution is to use sector decomposition to separate parameter space such that different pole rotation schemes can be applied in different sectors. This has been only partially investigated but with some success.

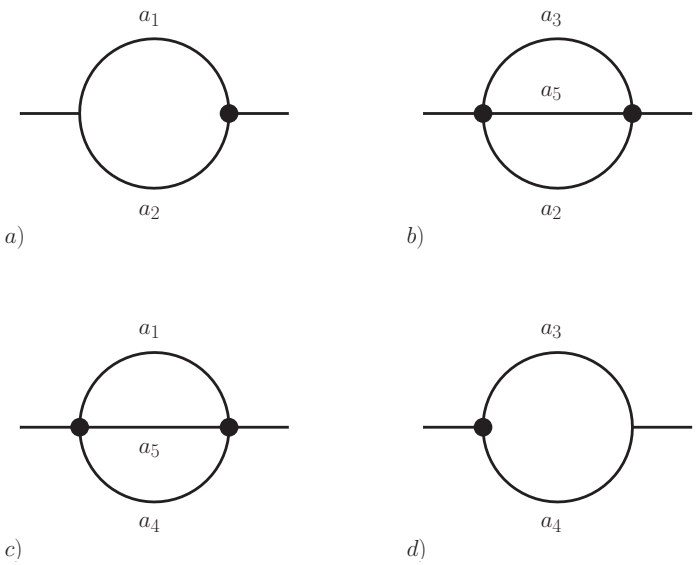

Figure 4.13: The four reduced graph for fig. 4.12. The thresholds occur at the following points in parameter space: a) at $\{2^{-1}, 2^{-1}, 0, 0, 0\}$; b) at $\{0, 3^{-1}, 3^{-1}, 0, 3^{-1}\}$; c) at $\{3^{-1}, 0, 0, 3^{-1}, 3^{-1}\}$ and d) at $\{0, 0, 2^{-1}, 2^{-1}, 0\}$.

Chapter 5

Real emission graphs

In chapter 3 we developed a technique to explicitly force the subtraction between a virtual integrand and its subtraction term before any integration took place. In this chapter we shall develop another technique to achieve the same for the real graphs. Our goal is twofold: where possible we wish to make the infrared cancellation manifest such that we only have to perform infrared finite integrals rather than compute the difference of multiple divergent ones; and secondly we must ensure that the sum of real-subtraction terms is equal to minus the sum of virtual-subtraction terms.

In two ways the calculation of the real emission graphs is easier than that of the virtual graphs. Firstly it is already well established that it is possible to perform point wise subtractions of infrared divergent quantities for the real emission graphs[1] [15]. Secondly it is always safe to presume that the momentum of the radiated massless particles is soft, if it was not the case then these particles would be detected and the amplitude would contribute to a different cross section with massless particles in the final state. This second feature of the real emission graphs will allow us to improve upon the point-wise cancellation technique by legitimizing the use of the Taylor expansion about the soft limit. This will allow us to drop the first order terms in the expansion as they will cancel, compute the second order terms which are finite and neglect higher order terms which are insignificant.

[1]Note that the real integrals are carried out directly in momentum space so there is no dubious parametrization issue

We have already seen that there is one major similarity between the infrared subtractions used in the virtual and the real emission graphs, namely that the massless propagators in the virtual subtractions have a very similar form as real emission phase-space terms. There also is a further similarity, the propagators that contribute to the infrared divergence in the virtual graphs are the same as those in the real graphs.

There are of course differences between the virtual subtractions and the real corrections. The overall momentum conserving delta function is necessarily different because there are different numbers of particles in the final state. The same logic also dictates that the experimental resolution function should also be different. Lastly there is no reason why the hard part of the matrix element in the real graph and its subtraction term need be indentical.

Of all the differences mentioned above the only one that will provide a serious challenge to compute is the difference of the momentum conserving delta functions. Essentially this is because it is not clear how to carry out analysis on distributions. Our strategy is to modify a generic real emission cross section such that all non-delta function differences between the cross section and its subtraction are removed § 5.2, this will then allow us to concentrate on the more difficult task of taking the difference of delta functions without any further complexity § 5.3. Invariably the hardest part of the calculation is the most interesting to perform and, pleasingly, it also has a very simple result § 5.3.2.

In appendix D we make some progress towards generalizing this result to multi-real emission graphs however this chapter is restricted to NLO graphs.

5.1 Next-to-leading order

For virtual graphs the IR divergence is found in the graph itself but for real graphs the IR divergence exists in the phase-space of the cross section. The real emission cross section σ is formed by considering the sum of all real emission graphs $\sum_i M_i$, fig. 5.1, and multiplying this sum against its own complex conjugate $\sum_j M_j^\dagger$. We then integrate over the appropriate phase-space between the two graphs which at NLO will be some hard particle phase-space, L_h, and one factor of $\delta^+(k^2)$ for the soft particle. There is also an overall momentum conserving delta function and

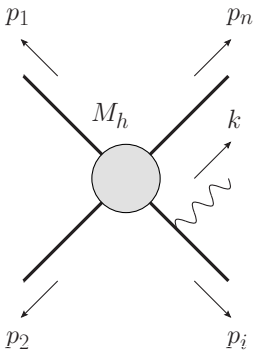

Figure 5.1: A generic NLO real emission graph. The soft particle with momentum k could radiate from any of the hard external legs $\{p_i\}$.

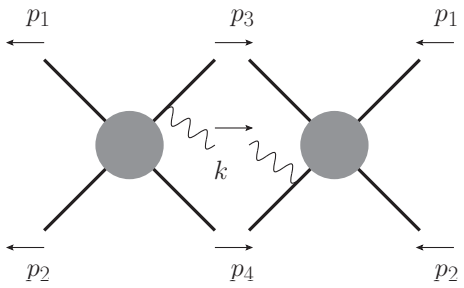

Figure 5.2: A generic NLO real emission with an s-matrix element squared proportional to $\frac{i}{2k\cdot p_3+i\epsilon}\frac{i^\star}{2k\cdot p_4+i^\star\epsilon}$.

the experimental resolution to consider. The partial real emission cross section $\sigma_{i,j}$ is the cross section obtained when just one of the many cross terms in the matrix element squared is considered,

$$\sigma_{i,j} = \int d^4k\; M_i(k)\, M_j^\dagger(k)\; \delta^+(k^2)\; \delta\left(\sum p + k\right)\; f(\{p\}, k). \tag{5.1}$$

$\{p\}$ is the set of all hard external momenta and $\sum p$ is shorthand for $\sum_i p_i$. For brevity we have omitted $\{p\}$ from M. The total real emission differential cross section is given by,

$$\sigma = \sum_i \sum_j\; \sigma_{i,j}. \tag{5.2}$$

We wish to work with $\sigma_{i,j}$ rather than σ so we can show finiteness of subtractions on a graph-by-graph basis. We shall factor the expression above into the

part that contributes to the soft behavior $S_{i,j}(k)$, the momentum conserving delta function, and the hard part $H_{i,j}(k)$. $H_{i,j}(k)$ is most easily defined by being the maximal part of the integrand that is well defined in the soft limit. Alternatively, at least at NLO, we see that,

$$S^{\pm}_{i,j}(k) = \delta^{\pm}(k^2)\ \frac{i}{2k\cdot p_i + i\epsilon}\ \frac{-i}{2k\cdot p_j + i\epsilon} \tag{5.3}$$

where the two propagators are contributed from M_i and $M_j^{\dagger}$, for example from fig. 5.2 we would obtain $S^{+}_{3,4}(k)$.

$$\sigma_{i,j} = \int d^4k\ H_{i,j}(k)\ S^{+}_{i,j}(k)\ \delta\left(\sum p + k\right) \tag{5.4}$$

5.1.1 Definition of the real-subtraction term

The generic form of the infrared subtraction which is equal and opposite to the virtual subtraction can be written in full generality as,

$$\mathrm{s}_{i,j} = \int d^4k\ h_{i,j}(k)\ S_{i,j}(k)\ \delta\left(\sum p\right). \tag{5.5}$$

There are three parts to this divergent integral. Firstly there is a hard part of the matrix element $h_{i,j}(k)$. $h_{i,j}(k)$ is not necessarily as that in the original real emission graph $H_{i,j}(k)$ because the subtraction used in the virtual and real graphs are also not necessarily the same. However $H_{i,j}(k)$ must have the same soft limit as $h_{i,j}(k)$ i.e. $h_{i,j}(0) = H_{i,j}(0)$. Secondly the soft part S is symmetric in the soft momentum's energy sign, $k \to -k$, i.e. $S = S^{+}/2 + S^{-}/2$. Lastly the momentum conserving delta function does not feature the soft massless particle's momentum k.

5.2 Partial subtraction of divergences

As stated in the introduction we shall proceed by modifying $\sigma_{i,j}$ until it is only distinguishable from $\mathrm{s}_{i,j}$ by the difference $\delta\left(\sum p + k\right) - \delta\left(\sum p\right)$. This is most easily achieved by performing the following two steps. First we add and subtract

the divergent integral $\mathrm{T1}_{i,j}$ from $\sigma_{i,j}$, where $\mathrm{T1}_{i,j}$ is defined as,

$$\mathrm{T1}_{i,j} = \int d^4k \; H_{i,j}(k) \; \frac{S^-_{i,j}(k)}{2} \; \delta\left(\sum p + k\right). \tag{5.6}$$

This leaves us with the following expression,

$$\sigma_{i,j} = \left[\frac{\sigma_{i,j}}{2} - \mathrm{T1}_{i,j}\right] + \left[\frac{\sigma_{i,j}}{2} + \mathrm{T1}_{i,j}\right] \tag{5.7}$$

$$= \int d^4k \; H_{i,j}(k) \left[\underbrace{\frac{S^+_{i,j}(k)}{2} - \frac{S^-_{i,j}(k)}{2}}_{\mathrm{sgn(k^0)S_{i,j}(k)/2}} + \underbrace{\frac{S^+_{i,j}(k)}{2} + \frac{S^-_{i,j}(k)}{2}}_{S_{i,j}(k)}\right] \delta\left(\sum p + k\right). \tag{5.8}$$

The odd function $\mathrm{sgn(x)} = \theta(\mathrm{x}) - \theta(-\mathrm{x})$ renders the first term finite in the soft limit. The soft part of the second term is now in the same form as $\mathrm{s}_{i,j}$, however the hard part is not because $H_{i,j} \neq h_{i,j}$[1]. Again we can add and subtract a second divergent term $\mathrm{T2}_{i,j}$ to remove the difference between the hard parts of the matrix element. This second term is defined as,

$$\mathrm{T2}_{i,j} = \int d^4k \; h_{i,j}(k) \; S_{i,j}(k) \; \delta\left(\sum p + k\right). \tag{5.9}$$

Adding and subtracting $\mathrm{T2}_{i,j}$ we have,

$$\sigma_{i,j} = \left[\frac{\sigma_{i,j}}{2} - \mathrm{T1}_{i,j}\right] + \left[\frac{\sigma_{i,j}}{2} + \mathrm{T1}_{i,j} - \mathrm{T2}_{i,j}\right] + \mathrm{T2}_{i,j} \tag{5.10}$$

$$= \int d^4k \; H_{i,j}(k) \; \mathrm{sgn(k^0)S_{i,j}(k)} \; \delta\left(\sum \mathrm{p} + \mathrm{k}\right)/2 \tag{5.11}$$

$$+ \int d^4k \; \left[H_{i,j}(k) - h_{i,j}(k)\right] \; S_{i,j}(k) \; \delta\left(\sum p + k\right) \tag{5.12}$$

$$+ \int d^4k \; h_{i,j}(k) \; S_{i,j}(k) \; \delta\left(\sum p + k\right) \tag{5.13}$$

We have already seen that the first term (5.11) in the expression above is finite in the soft limit. We now see that the second term (5.12) is also finite because

[1] Unless of course the real and virtual subtraction terms really are the same in which case $H_{i,j}(k) = h_{i,j}(k)$ and this step is trivial.

$H_{i,j}(0) = h_{i,j}(0)$. We are now in a position to subtract the actual subtraction term $s_{i,j}$,

$$\sigma_{i,j} - \mathrm{s}_{i,j} = \left[\frac{\sigma_{i,j}}{2} - \mathrm{T1}_{i,j}\right] + \left[\frac{\sigma_{i,j}}{2} + \mathrm{T1}_{i,j} - \mathrm{T2}_{i,j}\right] + [\mathrm{T2}_{i,j} - s_{i,j}] \tag{5.14}$$

$$= (5.11) + (5.12)$$

$$+ \int d^4k \; h_{i,j}(k) \; S_{i,j}(k) \; \left[\delta\left(\sum p + k\right) - \delta\left(\sum p\right)\right] \tag{5.15}$$

5.3 Subtraction of the delta function

Before we proceed it should be noted that what we are attempting to perform is a variation on Hadamard's procedure. For the virtual graphs we had a divergent generalized function (massless propagator) which we regulated by subtracting a constant from its test function, whereas for the real graphs we apparently have a divergent test function (the soft function is infinitely differentiable) which we are regulating by subtracting a distribution from another distribution.

At first sight it also appears that we cannot take the difference analytically as we did for the virtual graphs. However if we suppose that the delta functions are analytic and we can Taylor expand the difference in the soft limit,

$$\delta\left(\sum p + k\right) - \delta\left(\sum p\right) = k \cdot \frac{\partial}{\partial k}\delta\left(\sum p + k\right)\Big|_{k=0} + \mathcal{O}(|k|^2), \tag{5.16}$$

then we see that the remainder terms are proportional to $|k|^2$ which is sufficiently small to kill the logarithmic divergence in the soft limit. Noting that the divergent terms cancel and that we can ignore terms of order $\mathcal{O}(k^2)$ we are just left with terms of $\mathcal{O}(k)$ which are finite,

$$\sigma_{i,j} - \mathrm{s}_{i,j} = (5.11) + (5.12)$$

$$+ \int d^4k \; h_{i,j}(k) \; S_{i,j}(k) \; k \cdot \frac{\partial}{\partial k}\delta\left(\sum p\right) \tag{5.17}$$

However we now have to address what exactly the derivative of the delta function is.

5.3.1 Integration-by-parts trick

As with all generalized functions (including the delta function's integral, the step function) the derivative of the delta function is defined by its effect on a suitably well defined test function ϕ. Because the delta function only has support on zero it is clear that the following must be true:

$$\int dx \, \frac{d}{dx} \left(\delta(x)\phi(x)\right) = 0 \tag{5.18}$$

and therefore using the method of integration-by-parts we can define the derivative of the delta function as follows [16]:

$$\int dx \, \phi(x) \left(\frac{d}{dx}\delta(x)\right) = -\int dx \, \left(\frac{d}{dx}\phi(x)\right) \delta(x). \tag{5.19}$$

Using this identity we can 'bounce' the derivative off the delta function in (5.17) and onto the rest of the function,

$$\begin{aligned} \sigma_{i,j} - \mathrm{s}_{i,j} = &\ (5.11) + (5.12) \\ &- \int d^4k \, \frac{\partial}{\partial k_\mu} \left[k_\mu h_{i,j}(k) \; S_{i,j}(k)\right] \; \delta\left(\sum p\right). \end{aligned} \tag{5.20}$$

Using the chain rule we can break the expression above into two further terms,

$$\begin{aligned} \sigma_{i,j} - \mathrm{s}_{i,j} = &\ (5.11) + (5.12) \\ &- \int d^4k \;\; S_{i,j}(k) \; k \cdot \frac{\partial}{\partial k} \left[h_{i,j}(k)\right] \; \delta\left(\sum p\right) && (5.21) \\ &- \int d^4k \; h_{i,j}(k) \; \left[d + k \cdot \frac{\partial}{\partial k}\right] \; S_{i,j}(k) \; \delta\left(\sum p\right) && (5.22) \end{aligned}$$

$d = \frac{\partial}{\partial k_\mu} k_\mu$ is equal to the number of dimensions 4. Clearly (5.21) is finite due to the presence of the extra k in the numerator which is sufficient to kill the logarithmic soft divergence, however it is far from clear what the result of (5.22) is.

5.3.2 Homogeneity of the soft structure

A homogeneous function of degree n is a function $f(x_i)$ satifying:

$$f(\alpha\, x_i) = \alpha^n\ f(x_i) \tag{5.23}$$

By differentiating both sides of the expression above with respect to α and setting $\alpha = 0$ we obtain Euler's Homogeneous Function theorem (5.24),

$$x \cdot \nabla\, f(x_i) = n\, f(x_i), \tag{5.24}$$

(5.3) is a homogeneous distribution of order $n = -4$

$$\begin{aligned} S(k) &= \frac{i}{2k\cdot p_1 + i\epsilon}\,\frac{-i}{2k\cdot p_2 - i\epsilon}\pi\delta(k^2) \\ S(\alpha\, k) &= \frac{i}{\alpha\, 2k\cdot p_1 + i\epsilon}\,\frac{-i}{\alpha\, 2k\cdot p_2 - i\epsilon}\pi\delta(\alpha^2\, k^2) \\ S(\alpha\, k) &= \alpha^{-4}\ S(k) \end{aligned}$$

so we can use (5.24) on (5.22), but as $d+n=0$ this term is identically zero, thus we are left with the following sum of finite integrals,

$$\begin{aligned} \sigma_{i,j} - \mathrm{s}_{i,j} &= (5.11) + (5.12) \\ &\quad - \int d^4k\ \ S_{i,j}(k)\ k\cdot\frac{\partial}{\partial k} h_{i,j}(k)\ \delta\left(\sum p\right), \end{aligned} \tag{5.25}$$

which are all infrared finite.

What we have shown is that we can manifestly reduce the difference between an arbitrary NLO real emission graph and a suitably defined subtraction term to the sum of three finite integrands of the form (5.11), (5.12) and (5.25) which are thus suitable for evaluation by Monte Carlo as claimed in the introduction.

Chapter 6

Conclusions

The purpose of this thesis is to investigate the possibility of using momentum space subtractions to remove the soft infrared divergences from graphs for the purposes of evaluating the full cross section numerically. There are three principal conclusions to draw.

Firstly in chapter 3 we introduced a new method called Lagrange Decomposition that breaks up a loop integrand into a sum of terms, some of which are finite, and some are not. By considering these terms as being part of an S-matrix element rather than a Green's function we have shown that the terms in Lagrange Decomposition correspond to 'one particle cuts' and that the sum of these cuts is equal to the real part of the S-matrix element. This allowed us to identify the cuts of massless propagators with the soft singularities and the cuts of the massive propagators with the finite remainder. We then made the integrand finite by subtracting the divergent terms. By summing up the remaining soft finite-terms we obtained an expression featuring only massive propagators which strongly suggest that this part of the original integrand must be finite.

In spite of the successes of Lagrange decomposition it is not immediately useful as a method for computing the finite parts of the finite integrand because it is incompatible with Feynman parameter methods. The Feynman Parameter identity relies upon the real part of the propagators being positive but this is not the case with our chosen method of decomposition. We stress that this is an issue with Feynman Parametrization not with identifying soft subtractions. There are alternative ways of evaluating loop integrals which could avoid this issue

altogether, such as performing the free loop momentum integration numerically as well, however the most fruitful approach so far as been to the modification of the Feynman Parameter method as done in chapter 4. By rotating the threshold poles in the complex plane we have shown how it is possible to perform the contour integration numerically without difficulty. Indeed both the real and imaginary parts of the amplitude have been recovered for the bubble, triangle and box graph. However the method remains restricted to a handful of examples rather than the general prescription required to handle the complex overlapping branch cuts obtained from Lagrange Decomposition.

Lastly we have noted that although the remaining soft divergent terms left over from Lagrange Decomposition must, by unitarity, cancel the real emission contributions in the soft limit, it is not guaranteed that this will happen efficiently, or indeed at all, by straightforward Monte Carlo because of the non-analytic nature of the delta function. In chapter 5 we show how to take the difference between delta functions such that the remaining integrand is manifestly soft finite. The homogeneous structure of the soft S-matrix element greatly simplifies the procedure for identifying the finite part of the integrand to simply differentiating the hard part of the S-matrix element.

In summary by considering the virtual and real contributions to the cross section as distributions we can appeal to the theory of Generalized Functions to provide a method known as Hadamard's procedure to remove soft divergences by means of local momentum space subtractions. Furthermore we have presented techniques for both the real and virtual graphs that give manifestly finite integrands. The evaluation of the virtual finite terms is an outstanding problem due to the presence of a complicated branch cut structure of the integrands. We have made progress to resolve this by deforming the singular structure in a manner consistent with the Feynman prescription that allows for direct numerical computation. More work is required to extend this method to allow the computation of the finite parts of the virtual integrals.

Chapter 7

Postscript: Virtual Slicing

In this chapter we present an alternative approach to the calculation of soft divergences in virtual graphs which is based on the successful phase-space slicing method used for real graphs.

Phase space slicing [18] provides a simple approach to calculating infrared divergent real emission contributions to cross sections. Phase space slicing works by separating the IR and non-IR (UV) regions of a real emission integral with a step function in the energy of the relevant massless particle. The renormalized UV part of an integral can be calculated numerically in four dimensions, whilst the IR part can be accurately replaced by the Eikonal approximation which is evaluated in n-dimensions. Not only is the Eikonal approximation easier to calculate than the full expression but it is common to more than one graph and more than one theory, for example the vertex correction in QED has, up to a trivial scalar factor, the same Eikonal approximation as box graph in ϕ^3 with one massless particle, as such we can calculate the IR part of one graph once and then recycle the result for other graphs and other theories.

We shall largely restrict this chapter to the analysis of the vertex function in ϕ^3, its integrand is given by (7.1),

$$I = \frac{1}{k^2 + i\epsilon} \frac{1}{k^2 + 2k \cdot p_1 + i\epsilon} \frac{1}{k^2 - 2k \cdot p_2 + i\epsilon}. \tag{7.1}$$

Our starting point is to decide how exactly we are going to partition the IR and and UV parts of the integral. We could use a step function in the same manner as the phase space calculation but this makes the analytic calculation of the virtual integral excessively difficult. Instead we use a smooth step function ϕ, and its complement, which we denoted by $\bar{\phi}$;

$$\phi(p) = \frac{-\lambda}{k^2 + 2k \cdot p - \lambda} \tag{7.2}$$

and,

$$\bar{\phi}(p) = \frac{k^2 + 2k \cdot p}{k^2 + 2k \cdot p - \lambda} \tag{7.3}$$

In a theory like QED there are always three propagators contributing to any virtual IR divergence: a massless propagator and two adjoining massive propagators that are on shell. The simplest example of this structure is illustrated given by (7.1). We have deliberately chosen ϕ such that $\bar{\phi}$ alters the pole structure of an IR divergent Feynman propagator by giving it a small mass λ. Furthermore this Feynman-propagator-like form of partition function means that it can be evaluated using standard techniques such as Feynman parametrization. Initially we shall assume that the regulating mass squared λ is real. In § 7.2 we shall investigate the possibility that λ could be imaginary and negative in accordance with the Feynman $i\epsilon$ prescription. Typically we shall combine various ϕ's to give a very specific partition, a product of ϕ's is denoted by Φ and its inverse by $\bar{\Phi}$.

$$\int d^{4-2\epsilon}k\, I = \underbrace{\int d^{4-2\epsilon}k\, I\Phi(k)}_{\text{IR - analytic function}} + \underbrace{\int d^{4}k\, I\, \bar{\Phi}(k)}_{\text{UV - numerical}} \tag{7.4}$$

The mass squared regulator introduced by Φ renders the UV part IR finite and as such it can be computed numerically in four dimensions using the methods we have already developed in chapter 4 for massive integrals. Our task in this chapter is to calculate the IR function which corrects the finite four dimensional numerical result in order to recover the full divergent n-dimensional calculation. The accuracy of the Eikonal approximation will depend upon the extent to which

Φ successfully separates the IR and UV regions.

This method differs from traditional mass regulation in two respects. Firstly we shall investigate various choices of Φ including, but not limited to, the simple mass regulator for the massless particle. Secondly we are not intending to use successively smaller values of λ to allow extrapolation to the limit $\lambda \to 0$ but rather we shall accept a relatively 'large' value of λ to facilitate a fast numerical calculation and then work out how to alter this 'wrong' numerical answer to become the right one by means of an analytic function.

7.0.3 A simple partition function.

For the following choice of Φ we obtain a particularly simple IR function (7.25) which shall prove instructive to derive explicitly.

$$\bar{\Phi}_{\text{simple}}(k) = \bar{\phi}(p_1)\bar{\phi}(-p_2)\bar{\phi}(0) \tag{7.5}$$

Alternative choices of $\bar{\Phi}$ give more complicated IR matching functions but their general form, and the method for deriving them, is no more complicated than used in this simple example. $\bar{\Phi}_{\text{simple}}$ alters the UV part of the vertex function (7.1) to become:

$$\begin{aligned} UV &= \int d^4k\, I\, \bar{\Phi}_{\text{simple}} \\ &= \int d^4k\, \frac{1}{k^2 - \lambda + i\epsilon} \frac{1}{k^2 + 2k\cdot p_1 - \lambda + i\epsilon} \frac{1}{k^2 - 2k\cdot p_2 - \lambda + i\epsilon}. \end{aligned} \tag{7.6}$$

There can be no clearer example of an IR divergent integrand being rendered finite as all propagators have now been given an extra mass λ.

7.0.4 Mass regulating partition

The usual mass regulator can be implemented,

$$\Phi(k) = \phi(0), \tag{7.7}$$

which results in the following IR finite UV integral,

$$\begin{aligned} UV &= \int d^4k\, I\, \bar{\Phi}_{\text{mass}} \\ &= \int d^4k\, \frac{1}{k^2 - \lambda + i\epsilon} \frac{1}{k^2 + 2k \cdot p_1 + i\epsilon} \frac{1}{k^2 - 2k \cdot p_2 + i\epsilon}. \end{aligned} \tag{7.8}$$

Although the resulting IR matching function (7.34) is less elegant than the simple example above this choice of $\bar{\Phi}$ can be verified against well known results [12].

7.0.5 Improved partitionn.

Finally we present a choice of Φ_{IR} that gives a complicated IR matching function. In this case our starting point is to formulate Φ rather than $\bar{\Phi}$ because our intention is to choose a partition that creates a realistic IR approximation rather than a UV function that is easy to calculate or obviously finite. In fact both the resulting analytic IR matching function (7.36) and the IR-finite UV function (7.13) are comparatively complicated.

$$\Phi_{\text{IR}}(k) = \phi(p_1)\phi(-p_2)\phi(0) \tag{7.9}$$

Here we have constructed Φ such that its restricts the integration region to be closely bound to the poles of the original integral, this can be written using

Feynman parameters as,

$$IR = \lambda^3 \int_0^1 dx\, dy\, dz \int d^4k \, \frac{1}{[k^2 - \lambda x + i\epsilon]^2} \times \frac{1}{[k^2 + 2k \cdot p_1 - \lambda y + i\epsilon]^2} \frac{1}{[k^2 - 2k \cdot p_2 - \lambda z + i\epsilon]^2}. \quad (7.10)$$

The integrand is suppressed by a factor of $\lambda^3/[k^2(k^2 + 2k.p_1)(k^2 - 2k.p_2)]$ which is small if any of k^2, $k^2 + 2k.p_1$ or $k^2 - 2k.p_2$ are greater than λ. because the integral is UV convergent the contribution to the integral from this region is small. Explicitly this partition implies that k^2, $k^2 + 2k \cdot p_1$ and $k^2 - 2k \cdot p_2$ are small with respect to λ, and by implication this also implies that $k \cdot p_1$ and $k \cdot p_2$ must also be small. Suppose we now consider the vertex in QED; this involves the same denominator as (7.1) and a numerator proportional to the following,

$$N^\mu = \gamma^\nu \left(\not{k} + \not{p}_1 + m\right) \gamma^\mu \left(\not{k} - \not{p}_2 + m\right) \gamma_\nu. \quad (7.11)$$

When we consider this numerator as part of a squared matrix element then the k part must be of the form k^2, $k \cdot p_1$ or $k \cdot p_2$ and so in the IR approximation we can drop these terms, provided that we have suitably renormalized the integral such that it is UV convergent, and reduce this function to a trivial scalar multiplication of the scalar case. We shall always assume that $\lambda \ll m^2$ in order to justify expansion in $\lambda = 0$.

$$N^\mu \to \gamma^\nu \left(\not{p}_1 + m\right) \gamma^\mu \left(-\not{p}_2 + m\right) \gamma_\nu \quad (7.12)$$

In principle we could go further and reduce the IR approximation to the full Eikonal approximation but in practice this is not any easier to calculate and we have already made significant progress in dropping the non-trivial part of the numerator.

The corresponding UV function for $\Phi_{\rm IR}$ is fairly complicated and not obviously

IR finite. $\bar{\Phi}_{\mathrm{IR}}$ is given by:

$$\bar{\Phi}_{\mathrm{IR}} = 1 - \phi(p_1)\phi(-p_2)\phi(0). \tag{7.13}$$

It is always easier to deal with $\bar{\phi}$ terms rather that $1 - \phi$ because it a) it can be trivially multiplied against its target propagator which reduces the number of terms to be evaluated, and b) its IR finiteness is manifest. To this end we rewrite (7.13) as,

$$\bar{\Phi}_{\mathrm{IR}} = 1 - (1 - \bar{\phi}(p_1))(1 - \bar{\phi}(-p_2))(1 - \bar{\phi}(0))$$

$$\begin{aligned}\bar{\Phi}_{\mathrm{IR}} = {} & \bar{\phi}(p_1) + \bar{\phi}(-p_2) + \bar{\phi}(0) \\ & - \bar{\phi}(p_1)\bar{\phi}(-p_2) - \bar{\phi}(p_1)\bar{\phi}(0) - \bar{\phi}(-p_2)\bar{\phi}(0) \\ & + \bar{\phi}(p_1)\bar{\phi}(-p_2)\bar{\phi}(0)\end{aligned}$$

The bottom line of the expression above is the same as $\bar{\Phi}_{\mathrm{simple}}$ (7.5) whilst the last term in the top line of the expression above is the same as the mass regulator $\bar{\Phi}_{\mathrm{mass}}$. Exactly how the other terms alter the original integrand such that it is IR finite should now be obvious. This expression can be readily evaluated as before using the usual techniques.

7.1 Calculation of the simple IR function

There is not a great deal of point in this method unless the calculation of the n-dimensional IR matching function is significantly easier than the computation of the full result and indeed this does turn out to be the case.

Rather than compute the IR function directly which has a rather complicated starting point it is simpler to rearrange (7.4) and compute the difference between the UV part and the full solution. This is not as pointless as it first appears because it turns out that there are dramatic cancellations between the UV and

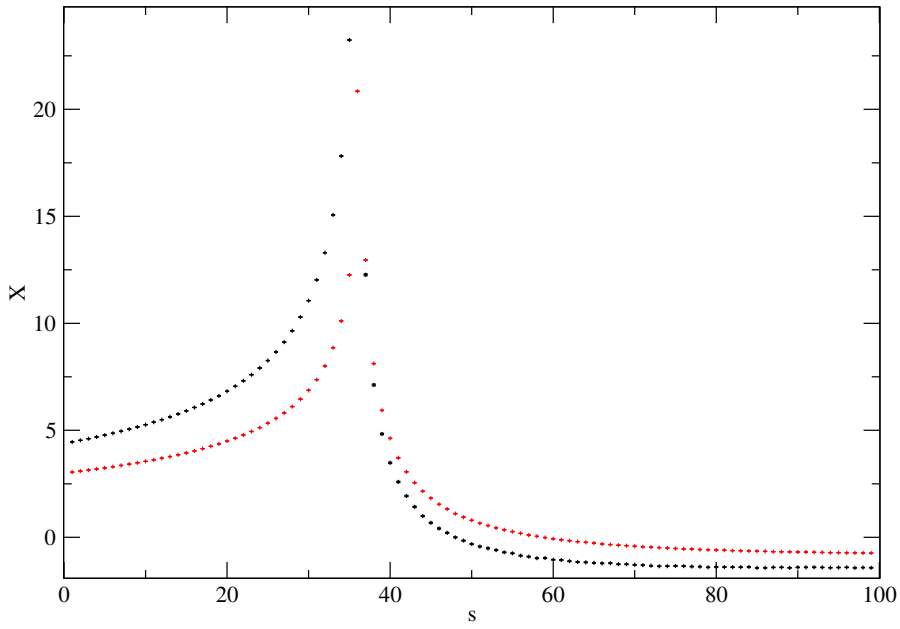

Figure 7.1: Results for different values of $\lambda = 0.1$ (red) and $\lambda = 0.01$ for the Real - UV part of vertex function the improved IR partition § 7.0.5, for $m = 3$.

the full solution which can be realized without having to work out either of them in full.

It is worth working out the full details of the calculation for Φ_{simple} because the method used certainly applies to the other choices of Φ discussed here and appears to be fairly general[1]. We begin with the dimensionally regulated expression for the original integrand (7.1),

$$I = \int d^{4-2\epsilon}k \, \frac{1}{k^2 + i\epsilon} \frac{1}{k^2 + 2k \cdot p_1 + i\epsilon} \frac{1}{k^2 - 2k \cdot p_2 + i\epsilon}. \tag{7.14}$$

We choose Feynman parameters such that the massless particle and the rest of the graph are conjoined with a single parameter y:

$$I = \int d^{4-2\epsilon}k \int_0^1 dx \int_0^1 dy \, \frac{2y}{[k^2 + 2k \cdot (p_1 x - p_2 \bar{x})y + i\epsilon]} \tag{7.15}$$

[1]We can also use this method for the box graph with two massless particles, the result is given in appendix C

where $\bar{x} = 1 - x$. Shifting $k \to k - (p_1 x - p_2 \bar{x})y$ we have,

$$I = \int d^{4-2\epsilon}k \int_0^1 dx \int_0^1 dy \, \frac{2y}{[k^2 - \Delta_x y^2 + i\epsilon]}. \tag{7.16}$$

where $\Delta_x = m^2 - sx\bar{x}$[1]. The corresponding UV part is trivially re-derived from the expression above by introducing λ. Because this integral is finite everywhere it is safe to set $n = 4$ from the beginning:

$$UV = \int d^4k \int_0^1 dx \int_0^1 dy \, \frac{2y}{[k^2 - \Delta_x y^2 - \lambda + i\epsilon]}. \tag{7.17}$$

Carrying out the virtual integration in both integrals we have:

$$I = -\frac{i}{(4\pi)^{2-\epsilon}}\Gamma(1+\epsilon) \int_0^1 dx \int_0^1 dy \, \frac{y}{[\Delta_x y^2]^{1+\epsilon}}. \tag{7.18}$$

and;

$$UV = -\frac{i}{(4\pi)^2} \int_0^1 dx \int_0^1 dy \, \frac{y}{[\Delta_x y^2 + \lambda]}. \tag{7.19}$$

In both cases the y integration is trivial[2],

$$I = -\frac{i}{(4\pi)^{2-\epsilon}}\Gamma(1+\epsilon) \int_0^1 dx \, \frac{1}{\Delta_x^{1+\epsilon}} \frac{1}{-2\epsilon}. \tag{7.21}$$

and;

$$UV = -\frac{i}{(4\pi)^2} \int_0^1 dx \, \frac{\ln(\Delta_x + \lambda) - \ln(\lambda)}{2\Delta_x}. \tag{7.22}$$

Because of the decision taken earlier to control the IR divergence with the single Feynman parameter y the IR part of the calculation is now essentially complete

[1] Δ_x can be small for $x(1-x) \approx m^2/s$. Near threshold, for example, $s \approx 4m^2$ and $x(1-x) \approx 1/4$ occurs for $x \approx 1/2$ (which is on the integration contour).

[2]
$$\int_0^1 dy \, y^{-1-2\epsilon} = \frac{1}{-2\epsilon} \int_0^1 dy \, \frac{d}{dy} y^{-2\epsilon} = \frac{1}{-2\epsilon} \left[y^{-2\epsilon}\right]_0^1 = \frac{1}{-2\epsilon}; \quad \epsilon < 0 \tag{7.20}$$

in so much that we can already identify the pole part and the finite part.

Expanding I about $\epsilon = 0$, and UV about $\lambda = 0$ we have,

$$I = -\frac{i}{(4\pi)^2}\int_0^1 dx\, \frac{-\epsilon^{-1} + \gamma - \ln(4\pi) + \ln(\Delta_x)}{2\Delta_x}, \tag{7.23}$$

and;

$$UV = -\frac{i}{(4\pi)^2}\int_0^1 dx\, \frac{\ln(\Delta_x) - \ln(\lambda) + \sum_{n=1}^{\infty}\frac{1}{n}\left(\frac{\lambda}{\Delta_x}\right)^n}{2\Delta_x}. \tag{7.24}$$

We have assumed that $|\Delta_x| > |\lambda|$ which is not necessarily the case, for example at threshold $s = 4\,m^2$, $|\Delta_x| = 0$ for $x = 1/2$, as such this result is invalid in this kinematic region. Now subtracting UV from I we see that the troublesome $\ln(\Delta_x)$ parts cancel, this is the most problematic part of the analytic calculation.

$$IR = I - UV = U + P_\lambda \tag{7.25}$$

The numerator of U is equal to the sum of the $\overline{MS}$ pole, $-\epsilon^{-1} + \gamma - \ln(4\pi)$ and $\ln(\lambda)$. P_λ is a power series in λ beginning at order λ. It is clear that U is the dominant part of the expression for small λ, interestingly it appears in all choices of Φ considered in this chapter. The numerical calculation of the UV part of the integral relies upon the existence of a small regulating mass λ if this is small then the Monte Carlo will struggle to converge to the correct result. By using the power series P_λ as well as the logarithmic part of the IR matching function we can afford to use a relatively large value of λ. Exactly how large λ can be will be examined in detail in § 7.1.1.

$$U = -\frac{i}{(4\pi)^2}\int_0^1 dx\, \frac{-\epsilon^{-1} + \gamma - \ln(4\pi) + \ln(\lambda)}{2\Delta_x} \tag{7.26}$$

$$P_\lambda = \frac{i}{(4\pi)^2}\int_0^1 dx\, \frac{\sum_{n=1}^{\infty}\frac{1}{n}\left(\frac{\lambda}{\Delta_x}\right)^n}{2\Delta_x} \tag{7.27}$$

The coefficients in power series in λ are easily[1] integrated with respect to x, the first few terms are:

$$P_\lambda = c_1\,\lambda + c_2\,\lambda^2 + \cdots \tag{7.28}$$

$$c_1 = g_s\left(\frac{1}{m^2} + 2\,s\,f_s\right) \tag{7.29}$$

$$c_2 = g_s\left(\frac{3}{2\,s} + \frac{1}{4\,m^4}\right) \tag{7.30}$$

where f_s and g_s are the ubiquitous kinematic functions,

$$f_s = \int_0^1 dx\,\frac{1}{2\Delta_x} = -\frac{\ln(x_s)}{s\sqrt{1-\frac{4\,m^2}{s}}} \tag{7.31}$$

and,

$$g_s = \frac{1}{4\,m^2 - s} \tag{7.32}$$

where we use the standard notation found in [2]

$$x_s = -\frac{1-\sqrt{1-\frac{4\,m^2}{s}}}{1+\sqrt{1-\frac{4\,m^2}{s}}} \tag{7.33}$$

7.1.1 Numerical results.

In fig. 7.2 we plot the percentage difference between the numerical method proposed in this section and the exact result obtained by [13] for the non-threshold kinematic variables $m = 3$ and $s = 4$. [2]. Comparing results obtained from using just the logarithmic correction, the $\mathcal{O}(\lambda)$ correction and the $\mathcal{O}(\lambda^2)$ correction we see that the logarithmic part of the correction dominates the result at small values of λ and the power series part dominates at $\lambda \sim 1$, whilst for $\lambda > 1$ the ap-

[1] 'Easily' means that they can be computed trivially using symbolic algebra software such as Maple.

[2] Using the $\overline{MS}$ prescription which absorbs the $\gamma - \ln(4\pi)$ term into the pole part ϵ^{-1} such that $\ln(\lambda)$ is the only surviving part of the numerator in U.

proximation is no longer valid and both the power series and the logarithmic part diverge rapidly. As expected the noise from the Monte Carlo routine becomes

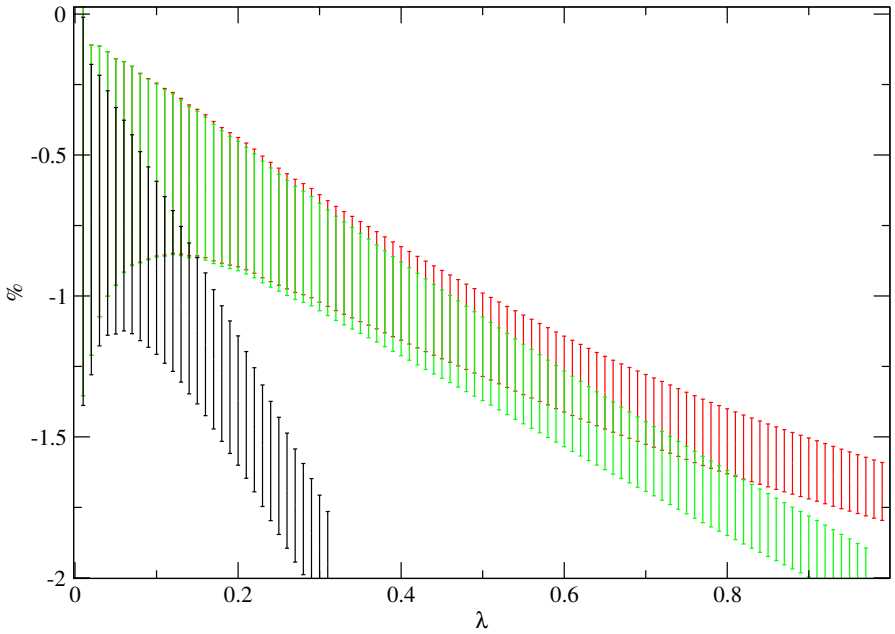

Figure 7.2: Results for different values of λ for the integration of the vertex function using the simple IR partition § 7.0.3, the y-axis gives the percentage difference in the numerical results from the exact result obtained from Ellis etc using a) just the logarithmic part of the IR function (black) b) the $\mathcal{O}(\lambda)$ approximation (green) and c) the $\mathcal{O}(\lambda^2)$ approximation (red) with 10,000 points using the GSL Vegas routine.

large as $\lambda \to 0$, and the power series increases the accuracy of the approximation for larger values of λ. It is not entirely clear from fig. 7.2 whether it is preferable to use a small value of λ for a more accurate approximation to the full result but with a larger error or a larger value of λ and tolerate a worse approximation for a smaller error. However if it is possible to increase the number of points used in the Monte Carlo then the error for all values of λ will improve whilst the power series approximation will not, as in fig. 7.3 which uses 10 times more points. In this graph we see that there is no clear increase in the error as $\lambda \to 0$ where as there is a clear increase in accuracy. Only for the very small values of λ does the failure of the Monte Carlo become evident as seen in fig. 7.4 where not only do both computations of 10,000 and 100,0000 points fail to accurately include the

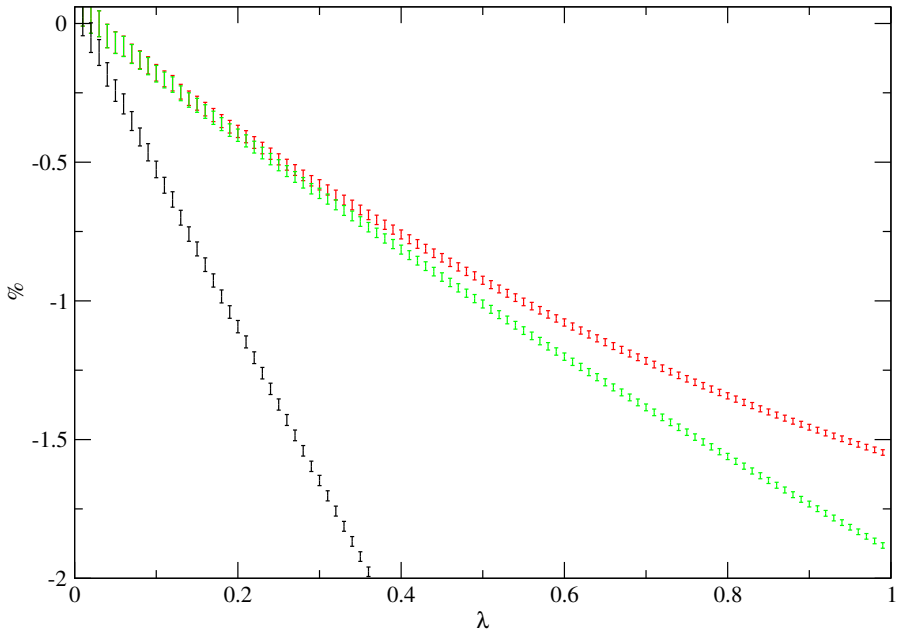

Figure 7.3: The same result as found in fig. 7.2 using 100,000 points in the GSL Vegas routine.

exact result within their errors but the 100,000 result is not even contained by the errors of the 10,000 result.

To obtain a level of accuracy of order 1% it is necessary to use very small values of λ where the power series has a negligible effect.

In fig. 7.4 we compare the results for small λ for 10,000 and 100,000 points. In order to push the accuracy of the method to an accuracy of order 0.1% it is necessary to use values of $0.004 < \lambda < 0.01$.

7.2 Imaginary λ

In this section we investigate the possibility of using an imaginary value of λ for the simple partition Φ_{simple} (7.5). This method essentially is an investigation into the possibility of using a non-zero value of $i\epsilon$, as a finite imaginary λ will make the $i\epsilon$ prescription irrelevant.

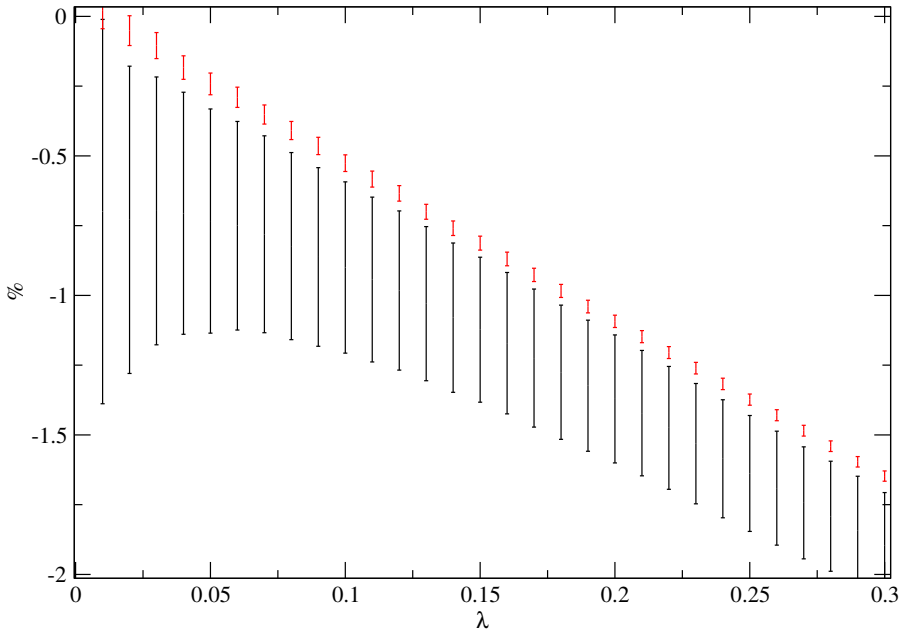

Figure 7.4: Comparison of 10,000 (black) and 100,000 (red) points in the GSL Vegas routine for small values of λ using the numerical result and the logarithmic correction.

There two reasons that suggest that an imaginary λ might be useful. Firstly a complex λ will provide us with the ability to compute and separate the real and imaginary parts of a complex integrand in the manner of chapter 4. Secondly if λ is purely imaginary then the first term in the power series correction (7.29) will also be purely imaginary and thus we can obtain a $\mathcal{O}(\lambda^2)$ level of accuracy by only using the second term in the power series correction (7.30) for the real part and the first term for the imaginary part. This suggests that the an imaginary λ will have better numerical behavior than an equivalent real valued λ.

7.2.1 Numerical results for imaginary λ

In fig. 7.6 we present the equivalents of figs. 7.2 and 7.3 for imaginary values of λ. Compared to the results for real λ we see that the $\mathcal{O}(\lambda^2)$ correction for imaginary λ provides a far more convincing correction to the logarithmic approximation even for large values of λ. Moreover if we plot the logarithmic parts of the UV functions for real and imaginary λ figs.7.8 and 7.7 then it becomes clear that

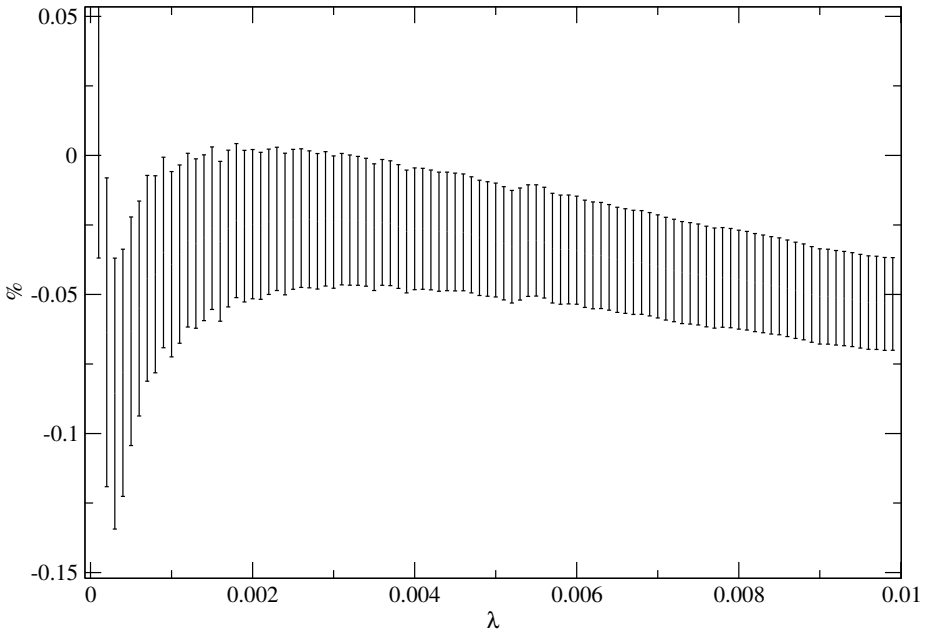

Figure 7.5: The results for small λ 100,000 points in the GSL Vegas routine, accuracy of order permille can be achieved for $0.004 < \lambda < 0.01$.

although the error for the two values of λ is comparable whilst the functional behavior for imaginary λ is far better than than for real λ

7.3 Calculation of analytically verifiable IR function

In the same manner as outlined above we obtain the following analytic result for the UV function using a mass regulator:

$$UV = -\frac{i}{(4\pi)^2}\int_0^1 dx\,\frac{\ln(\Delta_x)-\ln(\lambda)}{2\Delta_x} + -\frac{i}{(4\pi)^2}\int_0^1 dx\,\frac{\arctan\left(\frac{2\Delta_x-\lambda}{\sqrt{4\Delta_x\lambda-\lambda^2}}\right)+\arctan\left(\frac{\lambda}{\sqrt{4\Delta_x\lambda-\lambda^2}}\right)}{\Delta_x\sqrt{4\Delta_x\lambda-\lambda^2}}$$

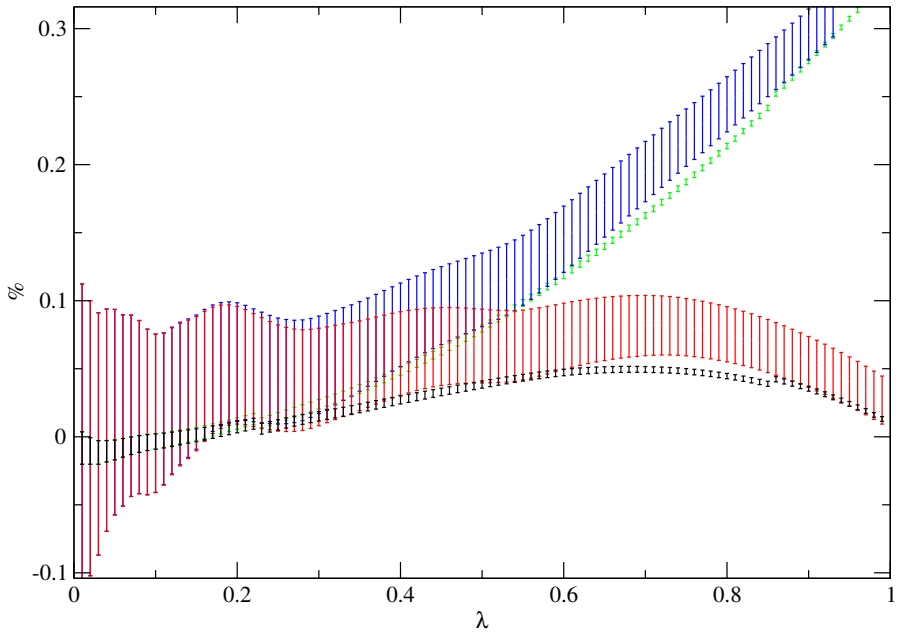

Figure 7.6: The percentage difference between the exact result and numerical value given for the logarithmic correction with 10,000 points (blue), 100,000 points (green), and the $\mathcal{O})(\lambda^2)$ correction with 10,000 points (red) and 100,000 points (black) for $0 < \lambda < i$ and $s = 4,\ m = 3$.

Subtracting this from the full result we again observe the cancellation of the dilogarithm terms and we have the same universal leading function and a different power series in λ

$$IR = U + c_1 \sqrt{\lambda}^1 + c_2 \sqrt{\lambda}^2 + c_3 \sqrt{\lambda}^3 + c_4 \sqrt{\lambda}^4 + \cdots \tag{7.34}$$

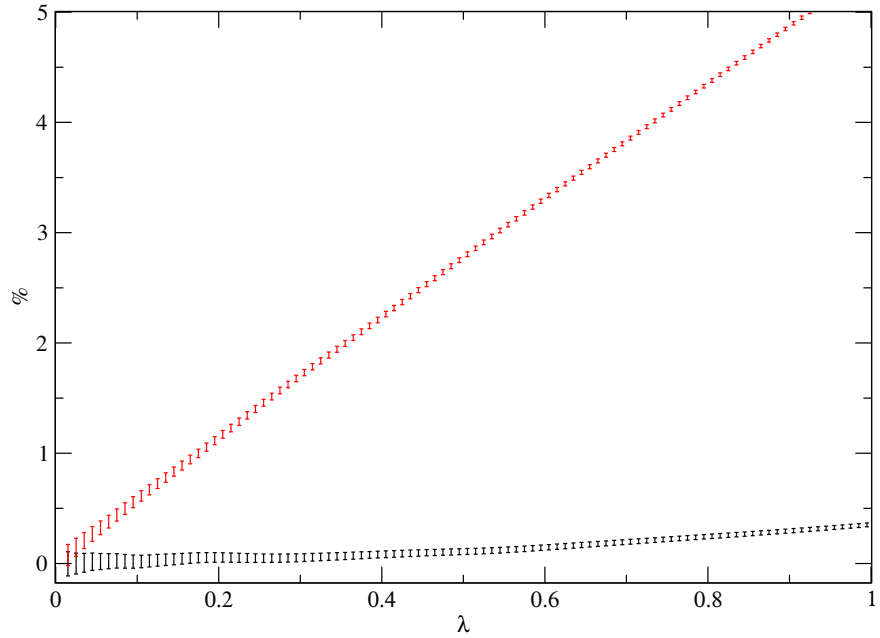

Figure 7.7: The results for real λ (red) and imaginary λ (black) using 100,000 points in the GSL Vegas routine.

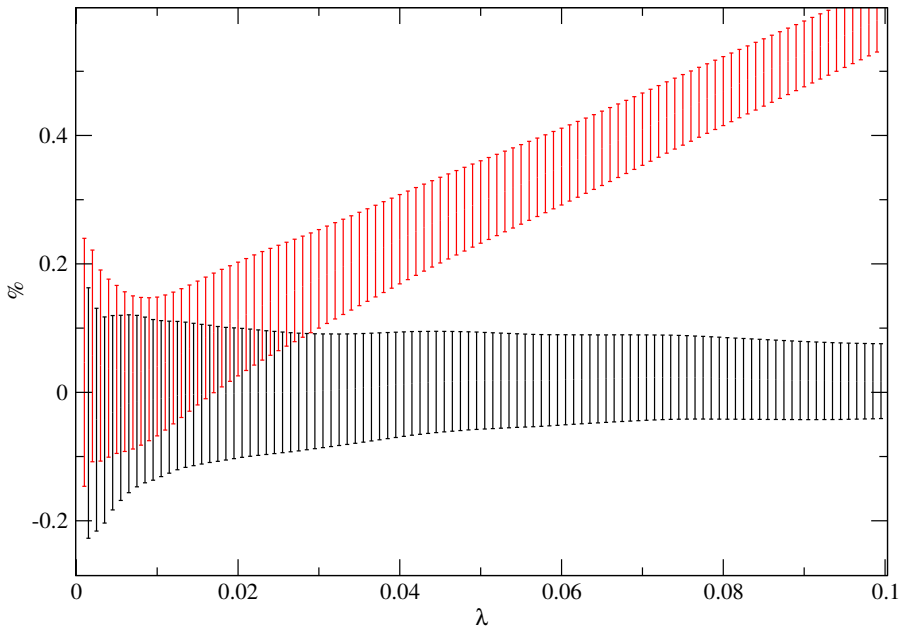

Figure 7.8: A close up of fig. 7.7. The results for real λ (red) and imaginary λ (black) using 100,000 points in the GSL Vegas routine.

where,

$$\begin{aligned} c_1 &= g_s \frac{\pi}{m^2} \\ c_2 &= -g_s \left(\frac{2}{m^2} - f_s \right) \\ c_3 &= c_1 \left(\frac{1}{24\, m^2} + \frac{g_s}{3} \right) \\ c_4 &= -\frac{c_2\, g_s}{2} \left(1 + \frac{1}{12\, m^2} \right) \end{aligned} \tag{7.35}$$

The analytic expressions for the dimensionally regulated vertex and the same vertex with a mass regulator[1] are well known and can be found in the appendices (B.5 and B.6) [12], taking the difference of these two expression we recover the function U.

7.4 Calculation of the improved IR function

The IR function for the improved $\bar{\Phi}_{\text{improved}}$, (7.13), is:

$$IR = IR_{\text{simple}} + c_0 + c_1 \sqrt{\lambda} + c_2 \sqrt{\lambda}^2 + c_3 \sqrt{\lambda}^3 + c_4 \sqrt{\lambda}^4 + \cdots , \tag{7.36}$$

where,

$$\begin{aligned} c_0 = {} & \frac{-i}{(4\pi)^2} \int_0^1 dx\, \frac{\ln(\Delta_x)}{2\, \Delta_x} \\ & + f_s\, \ln(\lambda) \\ & + \frac{2\, \mathrm{Li}_2(x_s^{-1}) - 2\, Li_2(x_s)}{s \sqrt{1 - \frac{4\, m^2}{s}}} \end{aligned} \tag{7.37}$$

[1] In the literature cited he expression for the mass regulator is only calculated up to the leading term in λ and the power series is neglected

The integrand in the first line of (7.37) is equal to the finite part of the full integrand (7.39) which is taken from [13]. This effectively makes this method redundant as it is easier to complete the full solution than it is to compute the IR matching function for this choice of Φ. For completeness the first terms in the power series are,

$$\begin{aligned} c_1 &= g_s \frac{2\pi}{m^2} \\ c_2 &= -g_s \left(\frac{1}{m^2} - \frac{1}{s}\right) - g_s f_s \left(\frac{2\,m^2}{s} + 1\right) \\ c_3 &= \frac{s^2\,\pi^2}{6\,m^2} g_s^4 \left(9\,m^2 - s\right) \\ c_4 &= -f_s\,g_s \frac{-7\,s^2 + 2\,m^4}{2\,s^2} + \frac{g_2^2}{12}\left(\frac{32}{m^2} + \frac{1}{s} + \frac{6\,m^2}{s^2} - \frac{3\,s}{m^4}\right). \end{aligned} \tag{7.38}$$

$$\begin{aligned} \int_0^1 dx\, \frac{\ln(\Delta_x)}{2\,\Delta_x} = \frac{x_s}{m^2\,(1-x_s^2)} \Bigg(&-\Gamma(\epsilon)\,\ln\left(\frac{4\pi\mu^2}{m^2}\right)\ln(x_s) - \frac{1}{2}\ln^2(x_s) \\ &+ 2\ln(x_s)\ln(1-x_s^2) - \frac{\pi^2}{6} + Li_2(x_s^2) + 2Li_2(1-x_s) + \mathcal{O}(\epsilon)\Bigg) \end{aligned} \tag{7.39}$$

7.5 Conclusions

The principal conclusion is that it is possible to evaluate Feynman integrals using a λ regulator and then recover the full result with an IR matching function.

However it is not always the case that the IR matching function is easier to compute than the full solution, this is obviously the case for the IR improved partition (7.13), in this case there is no point in pursuing this approach.

Perhaps the main achievement of this has been the method used to derive the simple partition function (7.25) which is very straightforward and has been replicated successfully for the double divergent box graph in appendix C. This method is similar to a traditional mass regulator except that it is somewhat easier to evaluate the Feynman integrals. Lastly we note that we can simplify

the method further by using the 'replacement rule', (4.13) [13],

$$\ln(\lambda^2) \to \frac{r_\Gamma}{\epsilon} + \ln(\mu^2) + \mathcal{O}(\epsilon) \tag{7.40}$$

which allows us to recover the soft divergence just from the λ regulated graph in 4-dimensions.

Should we use this λ regulating method then it is preferable to use an imaginary value of λ which gives a better numerical approximation to the full result for relatively large values of λ.

Appendix A

Alternative proof of the Largange identity (3.10)

This is in fact the original proof of (3.10) before the connection to Lagrange polynomials was realised, its nature is somewhat 'brute force' but unlike the proof given in the text it doesn't rely on any additional concepts such as polynomial interpolation.

We begin by recognizing that (3.10) trivially holds for $n = 1$. Assuming that (3.10) holds for some n we shall show that this implies that it must also hold for $n + 1$. To do this we firstly we write (3.10) for $n + 1$ and expand as a sum from $i = 1..n$ and an $i = n + 1$th term,

$$\sum_{i=1}^{n+1} \frac{1}{A_i} \prod_{j \neq i}^{n+1} \frac{1}{A_j - A_i} = \sum_{i=1}^{n} \frac{1}{A_i} \prod_{j \neq i}^{n+1} \frac{1}{A_j - A_i} + \frac{1}{A_{n+1}} \prod_{j \neq n+1}^{n+1} \frac{1}{A_j - A_{n+1}}$$

likewise the first product in the r.h.s can be written as a product of $j = 1..n$ and

a $n+1$th term. The second product can be trivially reduced to $j = 1..n$.

$$\sum_{i=1}^{n+1} \frac{1}{A_i} \prod_{j\neq i}^{n+1} \frac{1}{A_j - A_i} = \sum_{i=1}^{n} \frac{1}{A_i} \frac{1}{A_{n+1} - A_i} \prod_{j\neq i}^{n} \frac{1}{A_j - A_i} + \frac{1}{A_{n+1}} \prod_{j=1}^{n} \frac{1}{A_j - A_{n+1}}$$

using the identity $\frac{1}{A_i} \frac{1}{A_{n+1}-A_i} = \frac{1}{A_{n+1}} \left(\frac{1}{A_i} - \frac{1}{A_i - A_{n+1}} \right)$ to rewrite the first term in the r.h.s. we see that,

$$\begin{aligned} \sum_{i=1}^{n+1} \frac{1}{A_i} \prod_{j\neq i}^{n+1} \frac{1}{A_j - A_i} = & \frac{1}{A_{n+1}} \sum_{i=1}^{n} \frac{1}{A_i} \prod_{j\neq i}^{n} \frac{1}{A_j - A_i} \\ & - \frac{1}{A_{n+1}} \sum_{i=1}^{n} \frac{1}{A_i - A_{n+1}} \prod_{j\neq i}^{n} \frac{1}{A_j - A_i} + \frac{1}{A_{n+1}} \prod_{i=1}^{n} \frac{1}{A_i - A_{n+1}}. \end{aligned}$$

Taking the first term on the r.h.s. onto the l.h.s.,

$$\begin{aligned} & \sum_{i=1}^{n+1} \frac{1}{A_i} \prod_{j\neq i}^{n+1} \frac{1}{A_j - A_i} - \frac{1}{A_{n+1}} \sum_{i=1}^{n} \frac{1}{A_i} \prod_{j\neq i}^{n} \frac{1}{A_j - A_i} \\ & \qquad = \frac{1}{A_{n+1}} \left(\sum_{i=1}^{n} \frac{1}{A_i - A_{n+1}} \prod_{j\neq i}^{n} \frac{1}{A_j - A_i} - \prod_{i=1}^{n} \frac{1}{A_i - A_{n+1}} \right) \end{aligned}$$

and for clarity we now write $B_i = A_i - A_{n+1}$ on the r.h.s.,

$$\begin{aligned} & \sum_{i=1}^{n+1} \frac{1}{A_i} \prod_{j\neq i}^{n+1} \frac{1}{A_j - A_i} - \frac{1}{A_{n+1}} \sum_{i=1}^{n} \frac{1}{A_i} \prod_{j\neq i}^{n} \frac{1}{A_j - A_i} \\ & \qquad = -\frac{1}{A_{n+1}} \left(\sum_{i=1}^{n} \frac{1}{B_i} \prod_{j\neq i}^{n} \frac{1}{B_j - B_i} - \prod_{i=1}^{n} \frac{1}{B_i} \right). \end{aligned} \tag{A.1}$$

Assuming that (3.10) holds for some n then a) the r.h.s. of (A.1) must vanish

and b) the second term in the l.h.s. must equal $\prod_{i=1}^{n+1} A_i$,

$$\sum_{i=1}^{n+1} \frac{1}{A_i} \prod_{j \neq i}^{n+1} \frac{1}{A_j - A_i} - \prod_{i=1}^{n+1} \frac{1}{A_i} = 0.$$

Thus if (3.10) holds for n then it must also hold for $n+1$, as it is true for $n = 1$ so it is true in general.

Appendix B

Proof of (3.24)

In § 3.5 we claimed that if we partitioned an arbitrary loop integral using LD as,

$$\prod_{i=1}^{n}\frac{1}{A_i}=\sum_{i=1}^{n}\frac{1}{A_i}\prod_{j\neq i}^{n}\frac{1}{A_j-A_i},$$

and then partially resummed the first m terms,

$$\sum_{i=1}^{m}\frac{1}{A_i}\prod_{j\neq i}^{n}\frac{1}{A_j-A_i}=\sum_{i=1}^{m}\underbrace{\frac{1}{A_i}\prod_{j\neq i}^{m}\frac{1}{A_j-A_i}}_{Q_n[A_i]}\prod_{k=m+1}^{n}\frac{1}{A_j-A_i} \tag{B.1}$$

then we would have an expression that looked like,

$$\sum_{i=1}^{m}\frac{1}{A_i}\prod_{j\neq i}^{n}\frac{1}{A_j-A_i}=\frac{N}{\prod_{i=1}^{m}Q_n(A_i)},$$

where N is some polynomial composed from various A_is. In this appendix we shall prove this result. We begin by defining an object[1] $F[A_1,A_2,....,A_m]$ which

[1] This comes from another interpolating polynomial concept 'divided differences'.

is defined recursively as,

$$F[A_1, A_2, ..., A_m] = \frac{F[A_2, ..., A_m] - F[A_1, A_2, ..., A_{m-1}]}{A_1 - A_m}.$$

For example for $F[A_1, A_2, A_3]$ in full is,

$$F[A_1, A_2, A_3] = \frac{F[A_2, A_3] - F[A_1, A_2]}{A_1 - A_3} = \frac{\frac{F[A_3]-F[A_2]}{A_2-A_3} - \frac{F[A_2]-F[A_1]}{A_1-A_2}}{A_1 - A_3}$$

Fully expanding the line above and collecting the terms in $F[A]$ we have,

$$F[A_1, A_2, A_3] = \frac{F[A_1]}{(A_2 - A_1)(A_3 - A_1)} + \frac{F[A_2]}{(A_1 - A_2)(A_3 - A_2)} + \frac{F[A_3]}{(A_1 - A_3)(A_2 - A_3)},$$

and in general,

$$F[A_1, A_2, ..., A_m] = \sum_{i=1}^{m} \frac{F[A_i]}{\prod_{j\neq i}^{m}(A_i - A_j)}$$

Note the duality between the line above and (B.1), this shows us how to write the partial sum of Hadamard subtractions as,

$$\sum_{i=1}^{m} \frac{1}{A_i} \prod_{j\neq i}^{n} \frac{1}{A_j - A_i} = Q_m[A_1, A_2, ..., A_m]$$

where,

$$Q_m[A_i] = Q_m(A_i) = \frac{1}{A_i} \prod_{j\neq i}^{m} \frac{1}{A_j - A_i},$$

and,

$$Q_m[A_1, A_2, ..., A_m] = \frac{Q_m[A_2, ..., A_m] - Q_m[A_1, ..., A_{m-1}]}{A_1 - A_m}.$$

The problem is complicated by the fact Q's are inverse polynomials, we can simplify the situation by writing Q as,

$$Q_m[A_1, A_2, ..., A_m] = \prod_{i=1}^{m} Q[A_i]\, P_m[A_1, A_2, ..., A_m], \tag{B.2}$$

where P is a polynomial,

$$P_m[A_i] = \prod_{j \neq i}^{m} \frac{1}{Q_m[A_j]},$$

and is also defined recursively by,

$$P_m[A_1, A_2, ..., A_m] = \frac{P_m[A_2, ..., A_m] - P_m[A_1, ..., A_{m-1}]}{A_1 - A_m}. \tag{B.3}$$

Because $P_m[A_i]$ and $P_m[A_j]$ are polynomials so is $P_m[A_i] - P_m[A_j]$ and if $i = j$ then $P_m[A_i] - P_m[A_j] = 0$ which means that $A_i - A_j$ is a factor of $P_m[A_i] - P_m[A_j]$ and that $P_m[A_i, A_j] = \frac{P_m[A_j] - P_m[A_i]}{A_i - A_j}$ is also a polynomial, in fact by (B.3) all stages in the recursion are polynomials so that in (B.2) the denominator structure is entirely given by $\prod_{i=1}^{m} Q[A_i]$ as claimed in (3.24).

Appendix C

Scalar box with two massive particles

The box integral is evaluated using the same method as in § 7.1. Because there are now two massless propagators it is necessary to evaluate the Feynman parameter integrals associated with both massless lines before the expansion in λ can be made, again the last parameter integral is then trivial to perform.

The solution given below is the same as that found in [13],

$$I_4 = -\frac{2}{m^2\,t}\,\frac{x_s\,\ln(x_s)}{1-x_s^2}\,\ln\left(\frac{\lambda}{t}\right) + \mathcal{O}(\lambda^{1/2})$$

Higher orders in λ can also be easily evaluated,

$$
\begin{aligned}
c_1 &= \frac{-4\,\pi}{s\,t\,\left(1-\frac{4\,m^2}{s}\right)}\sqrt{\frac{\lambda}{m^2}} \\
c_2 &= \frac{8\,\arctan\left(\frac{s}{\sqrt{s(4\,m^2-s)}}\right)\left(\left(\ln\left(\frac{\lambda}{t}\right)+1\right)(4\,m^2-s+t)+t\right)}{\sqrt{s}\,t^2\,\left(4\,m^2-s\right)^{3/2}}\,\lambda \\
&\quad + \frac{2\,\left(\ln\left(\frac{\lambda}{t}\right)+2\right)}{(4\,m^2-s)\,t\,m^2}\,\lambda.
\end{aligned}
$$

Appendix D

Multiple emission graphs

The full generalization of the NLO real subtraction is beyond the scope of this thesis but we can make some progress towards this goal by showing how the method above can be used to remove the maximally divergent soft singularities for a given process.

The reason why it is so difficult to consider an arbitrarily complex real emission graph is the overlapping nature of the infrared divergences, however we can greatly simplify the situation by considering the Eikonal approximation where we replace a general massive propagator $\frac{i}{(k_1+...k_i+p)^2-m^2+i\epsilon}$ with $\frac{i}{2(k_1+...+k_i)\cdot p+i\epsilon}$ where $k_1 + ... + k_i$ is the sum of some soft radiated momenta. It has been shown [24] that the sum of all real emission graphs at the same order η in the Eikonal approximation is equal to,

$$\sigma_\eta = \int d^4k_1...d^4k_\eta \; H(\{k\}) \; \prod_i^\eta S^+(k_i) \; \delta\left(\sum p + \sum k\right) \tag{D.1}$$

where $\{k\}$ is the set of soft momenta and $\sum k$ is shorthand for $\sum_i^\eta k_i$. Interestingly the identity used to show this is identical to that of the momentum space representation of Sector Decomposition (3.39) by setting $A_i = 2p \cdot k_i + i\epsilon$.

As with the NLO case we can add and subtract terms from σ_η to get it into

the following form,

$$\begin{aligned}\sigma_\eta = &\text{ infrared finite terms} \\ &+ \int d^4k_1 ... d^4k_\eta \; h(\{k\}) \; \prod_i^\eta S(k_i) \; \delta\left(\sum p + \sum k\right)\end{aligned} \tag{D.2}$$

such that when we subtract the infrared limit, s_η, the only difference between it and (D.2) is in the momentum conserving delta function,

$$\begin{aligned}\sigma_\eta - \mathrm{s}_\eta = &\text{ infrared finite terms} \\ &+ \int d^4k_1 ... d^4k_\eta \; h(\{k\}) \; \prod_i^\eta S(k_i) \; \left[\delta\left(\sum p + \sum k\right) - \delta\left(\sum p\right)\right]\end{aligned}$$

Taylor expanding the difference of delta functions we get,

$$\begin{aligned}\sigma_\eta - \mathrm{s}_\eta = &\text{ infrared finite terms} \\ &+ \int d^4k_1 ... d^4k_\eta \; h(\{k\}) \; \prod_i^\eta S(k_i) \; \sum_j^\eta k_j \cdot \frac{\partial}{\partial k_j} \delta\left(\sum p\right)\end{aligned}$$

Applying the integration-by-parts technique as before we get,

$$\begin{aligned}\sigma_\eta - \mathrm{s}_\eta = &\text{ infrared finite terms} \\ &- \int d^4k_1 ... d^4k_\eta \; \sum_j^\eta \frac{\partial}{\partial k_j} \left[k_j \; h(\{k\}) \; S(k_j)\right] \; \prod_{i \neq j}^\eta S(k_i) \delta\left(\sum p\right).\end{aligned}$$

We now see that there are η copies of the NLO homogeneous distribution result which removes all derivatives of the soft structure to leave us with the following,

$$\begin{aligned}\sigma_\eta - \mathrm{s}_\eta = &\text{ infrared finite terms} \\ &- \int d^4k_1 ... d^4k_\eta \; \sum_j^\eta \left[k_j \cdot \frac{\partial}{\partial k_j} h(k_j)\right] \; \prod_i^\eta S(k_i) \delta\left(\sum p\right).\end{aligned}$$

This technique will but only work if $h(\{k\}) = h(\{0\})$ such that the derivative of the hard part is identically zero.

Bibliography

[1] Charalampos Anastasiou, Stefan Beerli, and Alejandro Daleo. Evaluating multi-loop Feynman diagrams with infrared and threshold singularities numerically. *JHEP*, 05:071, 2007. 28

[2] W. Beenakker and Ansgar Denner. Infrared divergent scalar box integrals with applications in the electroweak standard model. *Nucl. Phys.*, B338:349–370, 1990. 67

[3] Zvi Bern, Lance J. Dixon, David C. Dunbar, and David A. Kosower. One-Loop n-Point Gauge Theory Amplitudes, Unitarity and Collinear Limits. *Nucl. Phys.*, B425:217–260, 1994. 5

[4] T. Binoth, J. Ph. Guillet, G. Heinrich, E. Pilon, and T. Reiter. Golem95: a numerical program to calculate one-loop tensor integrals with up to six external legs. *Comput. Phys. Commun.*, 180:2317–2330, 2009. 5

[5] T. Binoth and G. Heinrich. An automatized algorithm to compute infrared divergent multi-loop integrals. *Nucl. Phys.*, B585:741–759, 2000. 32

[6] F. Bloch and A. Nordsieck. Note on the radiation field of the electron. *Phys. Rev.*, 52(2):54–59, Jul 1937. 4, 9

[7] N. Bogoluibov and O. Parasiuk. ber die multiplikation der kausalfunktionen in der quantentheorie der felder. *Acta Mathematica*, 97:227–266, 1957. 10.1007/BF02392399. 5

[8] William E. Caswell and A. D. Kennedy. Simple approach to renormalization theory. *Phys. Rev. D*, 25(2):392–408, Jan 1982. 6

[9] S. Catani and M. H. Seymour. A general algorithm for calculating jet cross sections in NLO QCD. *Nucl. Phys.*, B485:291–419, 1997. 4

[10] S. Coleman and R. E. Norton. Singularities in the physical region. *Nuovo Cim.*, 38:438–442, 1965. 35

[11] R. E. Cutkosky. Singularities and discontinuities of Feynman amplitudes. *J. Math. Phys.*, 1:429, 1960. 13, 35

[12] Stefan Dittmaier. Separation of soft and collinear singularities from one-loop N-point integrals. *Nucl. Phys.*, B675:447–466, 2003. 61, 74

[13] R. Keith Ellis and Giulia Zanderighi. Scalar one-loop integrals for QCD. *JHEP*, 02:002, 2008. 5, 41, 44, 46, 67, 75, 76, 83

[14] R. P. Feynman. Space-time approach to non-relativistic quantum mechanics. *Rev. Mod. Phys.*, 20(2):367–387, Apr 1948. 1

[15] S. Frixione, Z. Kunszt, and A. Signer. Three jet cross-sections to next-to-leading order. *Nucl. Phys.*, B467:399–442, 1996. 4, 48

[16] Israel Moiseevich Gel'fand and Georgi Evgen'evich Shilov. *Generalized Functions*, volume 1. Academic Press, 1964. 24, 54

[17] G. Grammer and D. R. Yennie. Improved treatment for the infrared-divergence problem in quantum electrodynamics. *Phys. Rev. D*, 8(12):4332–4344, Dec 1973. 4

[18] B. W. Harris and J. F. Owens. The two cutoff phase space slicing method. *Phys. Rev.*, D65:094032, 2002. 4, 58

[19] Klaus Hepp. Proof of the Bogoliubov–Parasiuk theorem on renormalization. *Commun. Math. Phys.*, 2:301–326, 1966. 5, 32

[20] A. D. Kennedy, Thomas Binoth, and Thomas Rippon. Automating renormalization of quantum field theories. In *SNC '07: Proceedings of the 2007 international workshop on Symbolic-numeric computation*, pages 18–27, New York, NY, USA, 2007. ACM. 6, 33

[21] Toichiro Kinoshita. Mass singularities of Feynman amplitudes. *J. Math. Phys.*, 3:650, 1962. 4

[22] Martin Lavelle and David McMullan. Collinearity, convergence and cancelling infrared divergences. *JHEP*, 03:026, 2006. 8, 9, 18

[23] Tsung-Dao Lee and Michael Nauenberg. Degenerate systems and mass singularities. *Phys. Rev.*, 133(6B):B1549–B1562, Mar 1964. 4

[24] Maurice Lévy and Joseph Sucher. Eikonal approximation in quantum field theory. *Phys. Rev.*, 186(5):1656–1670, Oct 1969. 85

[25] J. H. Lowenstein and E. Speer. Distributional limits of renormalized feynman integrals with zero-mass denominators. *Commun. Math. Phys.*, 47:43–51, 1976. 28

[26] Zoltan Nagy and Davison E. Soper. Numerical integration of one-loop Feynman diagrams for N- photon amplitudes. *Phys. Rev.*, D74:093006, 2006. 4, 35

[27] G. Passarino and M. J. G. Veltman. One Loop Corrections for e+ e- Annihilation Into mu+ mu- in the Weinberg Model. *Nucl. Phys.*, B160:151, 1979. 5

[28] R. J. Eden, P. V. Landshoff, D. I. Olive, J. C. Polkinghorne. *The Analytic S-matrix*. Cambridge University Press, 1966. 37

[29] A. Gehrmann-De Ridder, T. Gehrmann, and G. Heinrich. Four-particle phase space integrals in massless qcd. *Nuclear Physics B*, 682(1-2):265–288, 2004. 5

[30] Vladimir A. Smirnov. Analytical result for dimensionally regularized massless on-shell double box. *Phys. Lett.*, B460:397–404, 1999. 5

[31] Gerard 't Hooft and M. J. G. Veltman. Scalar One Loop Integrals. *Nucl. Phys.*, B153:365–401, 1979. 5, 8

[32] Gerardus 't Hooft and Martinus J G Veltman. *Diagrammar*. CERN, Geneva, 1973. 16

[33] J. B. Tausk. Non-planar massless two-loop Feynman diagrams with four on-shell legs. *Phys. Lett.*, B469:225–234, 1999. 5

[34] Inc Wolfram Research. Mathematica 7.0. *Champaign, Illinois*, 2008. 8

[35] D. R. Yennie, S. C. Frautschi, and H. Suura. The infrared divergence phenomena and high-energy processes. *Annals of Physics*, 13(3):379 – 452, 1961. 4

[36] W. Zimmermann. Convergence of bogoliubov's method of renormalization in momentum space. *Communications in Mathematical Physics*, 15:208–234, 1969. 10.1007/BF01645676. 5